Electrical Textile Valves for Paper Microfluidics

WILEY-VCH

DOI: 10.1002/ adma.201702894
Article type: Communication

Electrical Textile Valves for Paper Microfluidics

*Alar Ainla, Mahiar M. Hamedi, Firat Güder, and George M. Whitesides**

Dr. A. Ainla, Dr. M.M. Hamedi, Dr. F. Güder, Prof. G. M. Whitesides
Department of Chemistry and Chemical Biology, Harvard University
Cambridge, MA
02138
USA

(*) Author to whom correspondence should be addressed:

E-mail: gwhitesides@gmwgroup.harvard.edu

Keywords: paper microfluidics, valves, electrowetting, textiles

Abstract

This paper describes electrically activated fluidic valves that operate based on electrowetting through textiles. The valves are fabricated from electrically conductive, insulated, hydrophobic textiles, but the concept could be extended to other porous materials. When the valve is closed, the liquid cannot pass through the hydrophobic textile. Upon application of a potential (in the range of 100 - 1000 Volts) between the textile and the liquid, the valve opens and the liquid penetrates the valve. These valves actuate in less than 1 second, require low energy (~27 μJ per actuation), and work with a variety of aqueous solutions, including low surface tension aqueous liquids, and bioanalytes. They are bistable in function, and are in a sense, the electrofluidic analog of thyristors. They can be integrated into paper microfluidic devices to make circuits that are capable of liquid control, including autonomous fluidic timers, and fluidic logic.

Paper microfluidics is a technology particularly well-suited for uses in public health, point of care diagnostics for resource-limited settings, veterinary medicine, food and water quality testing, and environmental monitoring.[1],[2],[3],[4],[5],[6],[7],[8] Many common assays require the addition of multiple reagents and multiple washing steps, where the timing of each step influences the outcome of the assay. For example, paper-based devices for ELISA[9,10],[11],[12], electrochemiluminescence (ECL)[13], or DNA detection[14],[15], require multiple individually timed steps of binding, washing and amplification. Performing these steps manually is labor intensive (a single assay may take from several minutes to hours) and prone to human errors. Fully automated paper-based assays have the potential to be faster and more accurate than those requiring human operations.

The most important component required for autonomous assays is a fluidic valve that gates the flow of liquids with timed actuation. Different methods of valving have been explored for paper devices[16],[17],[18],[19],[20],[21],[22],[23], which operate either by changing the wicking properties of the paper or by mechanically altering connectivity between the channels. Wicking speed in the paper is determined by three parameters: The hydrophilicity of its surface, the size of the pores, and the viscosity of the liquid. These parameters can be altered to actuate flow of liquids. For example, hydrophobic surfaces can be rendered hydrophilic by an electrical plasma[16] or by electrochemical[17,24] or ultraviolet modification.[25] Surfactants can also be used to assist liquids in crossing the hydrophobic barriers[23,26,27]; dissolved polymers[28] or sugars[29] can increase the viscosity of the liquids and limit the flow.

Mechanical motion of paper has also been used for actuating the flow of liquids in paper. Electromagnetic[18], hygroexpanding[19],[30] manually operated push-buttons[20], flaps[21], pop-up[31], folding[10],[32] and sliding strip[14] concepts for valving have been reported in the

literature (for a more complete list of published work see Table S1). Valves that involve soluble substances, such as surfactants, or chemical modifications, like plasma, or electrochemistry, are more prone to influence the reagents used in the assays compare to purely physical methods, such as mechanical motion. Mechanical valves, such as manually operated push-buttons or cantilevers do not have this drawback, but mechanical parts are more prone to failure than chemical, and they cannot be controlled using simple electronics.

This manuscript describes an electrically actuated valve based on a fine electroactive mesh or textile fabricated from woven fibers whose wettability can be controlled by application of a voltage (**Figure 1**). We call this mesh an "electrotextile" and describe its fabrication and properties below.

Electrotextile-based valves have four characteristics that have the potential to be useful in paper devices: i) They are controlled electronically (e.g., they require no mechanical parts). ii) They are simple and inexpensive to fabricate. iii) They can be integrated with paper microfluidics. iv) They operate rapidly (i.e. they actuate in < 1s).

We show that this new class of valves can be integrated into paper microfluidic devices, and use the valves as a building block for fabricating devices of higher complexity such as circuits that contained valves in series and parallel configuration. We also demonstrated circuits with timed actuation and a self-regulation (i.e. logic NAND gate) for fluidic logic. We also constructed a battery-operated, portable control unit for the actuation of the valves using off-the-shelf electronics.

To characterize the electrowetting in the electrotextile valves, we used woven textiles that contain metallic fibers or plastic fibers having a conductive metal coating. We also explored conductive paper (SI and Table S2) but concluded that electrotextiles were easier to prepare and more consistent in their performance. All the materials were coated with Parylene-C[33,34] for electrical insulation between the liquid and the metal, and Teflon AF[35], to increase the hydrophobicity of their surfaces (see **Table 1**).

We measured the breakthrough pressure of water through different electrotextiles using a simple device in which we increased the applied pressure by increasing the height of a column of water, placed on top of the textile until the valve opened (without using electrical actuation; see Figure S1). We found that the breakthrough liquid pressure was in the range of 6-12 mbar (0.6-1.2 kPa) for the materials that we tested (see Table 1 and S2). We then investigated the voltage threshold for actuation for the different materials, using deionized water (see experimental details, and Figure S3); we determined that a potential between 100-1000V activated all of the different electrotextiles. The breakthrough pressure of the hydrophobic textiles was sufficiently high to allow containment of liquids for applications in microfluidics.

This valve is bistable. Once a flow is initiated due to electrowetting, it cannot be stopped until the entire volume of liquid flows across. We confirmed the bistable character of the valve by running several (up to five) actuation cycles in series. For each cycle, we deposited a drop of liquid onto the electrotextile valve. The liquids did not pass the valve until an actuation pulse of 300V for 0.5s was applied (Figure S7-S8). The flow of liquid continued until the entire drop passed through the valve (i.e. well after pulse had ended). After 30-45s (after the flow had ceased), the valve dried, and the cycle could be repeated.

To understand the behavior of electrowetting through electrotextiles better, we developed a theoretical model for the operation of this new class of valves, inspired by the principles of electrowetting-on-dielectric (EWOD).[36–48] EWODs have been widely studied and used in the field of “digital microfluidics" for handling of liquids on planar surfaces. In our case, however, the valves do not have planar surfaces and instead operate based on the principle of penetration of liquids through porous materials with the help of electrowetting. (This type of materials has not -- to our knowledge -- been used previously for microfluidics). To describe this complex process with a simple model, we combined the Washburn equation[49] with the Lippmann-Young equation for EWODs[46], and derived an analytical

expression (Equation 1; see the SI for details) for the activation voltage U_a required to trigger flow of liquid through the electrotextile.

$$U_a = \sqrt{-\frac{2\sigma d_i cos\theta_0}{\varepsilon\varepsilon_0}} \quad (1)$$

Here, θ_0 is the stationary contact angle of water on planar surface of the electrotextile material (Teflon-AF), ε is the dielectric permeability of the layer of insulation on the wires (3.15 for Parylene-C), d_i is the thickness of the insulation layer (~10μm Parylene-C), and σ is surface tension of the liquid.

To test this theory, we used mixtures of ethanol (EtOH) and water to vary the surface tension of the liquid σ_i= *72mN/m (water), 56 mN/m (5% EtOH), 48 mN/m (10% EtOH), 28 mN/m (50% EtOH)* , and measured the actuation voltage for each liquid using an aluminum electrotextile coated with Parylene-C (11 μm), and Teflon AF (see **Table 2**). As expected, the actuation voltage decreased with lower surface tension (according to Equation 1). Interestingly, the standard deviation of the actuation voltage also decreased monotonously with decreasing surface tension. Equation 1 can estimate the voltage for actuation for different materials and liquids, and describe the trends, but does not provide exact numbers (see SI, and Figure S4). To describe electrowetting through textiles, we believe that an improved theory would be useful – one in which the Lippmann-Young equation is replaced with a model that fits the three-dimensional microscale geometries used here. A more accurate model than the Washburn equation would describe the pressure required for a liquid to penetrate the textile.

We also used the aluminum electrotextile (Table 2) to determine the valving behavior for solutions with different compositions (which may be relevant in various bioanalytical assays). We tested solutions of Pluronic® F-68 which is an example of a surfactant used in some bioassays. The use of surfactant reduced the actuation voltage and the standard deviation. We tested solutions of bovine serum albumin (BSA), as an example of a protein-

containing solution. The BSA solutions penetrated through the valve upon actuation with actuation voltages similar to that of water, and demonstrated that the higher viscosity does not affect electrowetting. We also tested human whole blood, which also actuated, showing that complex bodily fluids, containing cells, can pass through the pores of the woven textile.

After having established that bistable valves can be fabricated using electrotextiles, we integrated the valves and other relevant components into paper microfluidic devices. This integration was achieved by stacking paper with microfluidic structures, with electrodes printed on its surface, together with electrotextiles, into multi-layer devices (see experimental details and **Figure 2** A).

The most basic components that can be implemented with this fabrication technique are printed electrodes/wires[50] and paper-based microfluidic channels.[51] By adding two more basic components, the electrical valve, and a fluid-to-electrical switch (this component switches an electrical signal using a liquid input), we could design and fabricate simple integrated circuits. In these circuits liquids and electrical signals could control each other interchangeably, so we term them "printed electrofluidic circuits". Because of the bistable nature of the valves, they are functionally analogous to semiconductor thyristors, which are devices used widely in AC power electronics (and not analogous to the transistors used much more widely in binary information processing). A thyristor switches “on” quickly when a voltage pulse is applied to its gate electrode and remains open as long as a positive electrical potential is present between the cathode and anode. Inspired by the electronic symbol for the thyristor, we have designed a symbol for the textile valve where the gate is an electrical conductor made of a solid material, and the anode and cathode are represented as fluidic channels. We call this an "electrofluidic thyristor" (Figure S7). Figure 2C shows the proposed circuit diagram symbol for all the electrofluidic components.

We integrated the electrofluidic switch and valves using these design principles (see Figure 2B): i) *A fluid-to-electrical switch.* We fabricated this switch by printing two carbon

electrodes separated by a microfluidic channel in between. When there is no electrically conducting liquid (e.g. aqueous solution) present in the channel, the dry paper does not allow flow of significant electrical current from one electrode to the other, essentially rendering the switch "off". Low currents are still possible due to spontaneous conductivity of paper[52], but in our observation, this conductivity is not sufficient for valve operation. The flow of larger electrical current is only possible when a liquid electrolyte is present in the channel, turning the switch "on". ii) *An electrofluidic valve*. The basic valve design consisted of a three-layer structure, where the electrotextile was sandwiched between two sheets of paper with wax-printed microfluidic structures (Figure 2). We printed carbon electrodes in the liquid reservoirs in the top layer, which acted as individual electrodes ("source") for each valve. The electrotextile in the middle layer was connected to ground ("gate"). Liquids placed in the reservoir do not penetrate through the middle layer until a voltage pulse is applied to activate the valve and allow the liquid to flow through to the bottom microfluidic layer.

The behavior of fluids in these valves is dominated by capillarity for the relatively small amounts of liquid volume that we use, and gravity should not have a large effect on the valving. To determine the effect of gravity we tested several paper devices at different angles vs. gravity (see methods). As expected the valves operated at all angles from 0˚ to 180˚ (upside down) and the activation voltage was independent of the angle (Supplementary Information and Figure S9).

The electrofluidic thyristor provides a building block that can be integrated into three-dimensional circuits in various configurations for applications involving paper microfluidics. Integrating these valves, in series or in parallel, allows fabrication of devices with a greater complexity.

Figure 3 demonstrates the integration of the valves in parallel. Here two valves were fabricated on the same layer. Each valve has an individual reservoir for liquid, and we could operate them individually and deliver each liquid to a common microfluidic channel. This

configuration, could allow the time-controlled addition of multiple solutions and reagents to an assay, as seen in Figure 3 D.

Figure 4 B and C shows serially connected valves fabricated using a five-layer configuration. This device uses two separate electrotextiles for each valve (in layer 2, and layer 4). It is essentially a vertical flow device, in which the first valve passes the fluid from layer 1 to layer 3, and the second valve passes the fluid from layer 3 to layer 5 (see Figure 4 D). Such architectures could be used for assays involving multistep reactions.

We show two examples of self-regulating electrofluidic paper chips. The advantage of such devices was that no external circuitry is required for controlling the timed signals. Instead the timing and logic functions and signals are generated in the paper device itself.

In the first example, we fabricated a fluidic timer ("fTimer"), shown in **Figure 5** A and B. We demonstrate this device because autonomous timing of liquids is important for many applications, and a number of approaches have already been demonstrated[23,27]. The fTimer device is activated when water is added to a microfluidic channel, (which acts as the timer). The liquid wicks along the channels at a speed determined by the properties of the paper and the fluid, and turns on a number of fluid-to-electrical switches along its path. Each switch triggers a valve and allows flow of three different liquids into a common output channel (Figure 5 C).

The second example demonstrates a logic flow-control, which would allow actuating the valve depending on simple binary input conditions, presence (logic state ‘1’) or lack (logic state ‘0’) of the liquid in the inputs. Our logic flow-control circuit performs Boolean NAND operation (we can call it also fluidic NAND gate, or simply fNAND). The NAND gate is the fundamental building block of all digital logic and any digital circuit element can be constructed using a combination of NAND gates alone. The difference between the fNAND and an electronic NAND is that the inputs and outputs of the fNAND are encoded by the presence of the fluid in channels, instead of electrical voltage between wires. The main

limitation of paper-based logic flow-control is that the state of each gate can be evaluated only once. Wicking is a one-way process and filling of paper channels is irreversible, which means that any given state can only transition from '0' to '1', but not vice versa. This requires that evaluation of the logic gate is triggered and output is only generated after a clocking signal (**Figure 6** A and S10 A). Corresponding equivalent in electronics would be NAND gate with output couple through a D flip-flop (Figure S10 B). D flip-flops copy their input (D) to output (Q) only during the rising-front (transition from '0' to '1') of clocking signal (CLK), while output remains unaffected during both the low and the high CLK states. Similarly, our fNAND gate has one output valve, which is triggered by the clock. The valve is not actuated only when both inputs (A and B) are in state '1' during the rising clock signal, since NOT ('1' AND '1') is '0'.

Paper microfluidics is most practical in settings where portability, simplicity of operation, and affordability, are crucial. We and others have proposed simple portable electronic devices that are capable of performing advanced electroanalytical tests on paper microfluidic devices.[53] The ability to control the valve with a simple, portable device is, therefore, important. Even though the valves require relatively high actuation voltage (up to 600V), we have constructed a simple electronic power supply with a cost of materials less than 10 USD that can be operated from a single 1.5V AA battery (Figure S11) and deliver the appropriate voltage. All the essential components of the power supply were extracted from a disposable photo camera. (Figure S11)

We calculated that the energy required for actuation of the valves is around 27μJ (the experimental requirements of energy were measured to be slightly higher due to leakage currents, but nonetheless less than 1mJ/actuation −see SI). The low power consumption is one of the advantages of the valves. A single battery could power many paper chips with our portable device (Estimated about 20,000 cycles, see figure S11 for details).

Finally, we demonstrated the valve in an iodate assay reported by Lieberman et al.[54] Briefly, this assay is composed of the analyte (KIO_3^-), three reagents (p-toluenosulfonic acid, KI, $Na_2S_2O_3$) and a starch indicator that produces the colorimetric output signal. In this assay, the excess iodide reacts with the iodate in the acidic environment and forms triiodide (Equation 2). Triiodide is then titrated with thiosulfate (Equation 3), If the amount of triiodide exceeds the reducing capacity of the thiosulfate the indicator starch turns blue (Equation 4), and if the amount of triiodide is smaller the indicator remains uncolored.

$$IO_3^- + 6H^+ + 8I^- \rightarrow 3I_3^- + 3H_2O \quad (2)$$

$$I_3^- + 2S_2O_3^{2-} \rightarrow 3I^- + S_4O_6^{2-} \quad (3)$$

$$I_3^- + starch \rightarrow blue\ complex \quad (4)$$

In this assay, the analyte and reagents should be mixed first and the product should be applied to the indicator area for evaluation in a timed manner. To integrate this assay in a paper device, we dried the reagents in different zones in an input pad (since the reagents are mutually incompatible). For mixing we place 40 µL of analyte on the input pad. This amount of liquid was sufficient to cover the entire input pad and connect the individual zones. Since paper could not absorb the entire volume in its pores, an open drop left outside of the paper matrix would support convective mixing upon mechanical agitation. For timing, we integrated a valve that was actuated 3 minutes after mixing to bring the product into an indicator pad, where a colorimetric output signal was generated (see **Figure 7**, and experimental section). The timing was controlled digitally in the voltage generator device, since we think it is feasible that paper devices would be interfaced with digital electronics (e.g. cell phones). It should however be easy to integrate a fluidic timer (similar to the device that we demonstrated in Figure 5) with the iodate assay for a more autonomous device that would only rely on a voltage source without any additional electronic circuitry.We designed the reagent concentrations for a test that would be useful for analyte concentration of around 1mM (see supporting information). Figure 7 C shows the results for 0, 1, and 5 mM analyte

concentrations tested using the integrated devices. Note that even the test with pure water shows a background color although no color signal is produced in paper. The reason is that a wet paper layer is more translucent making the darker gate mesh visible in the signal. Tests with indicator pads, which do not have the gate mesh do not show this background. This problem could be addressed by designing a white gate mesh. The iodate assay shows the possibility of integrating valves into paper-based assays, and we envision that other assays (which may even require several timing steps, and thus several valves), can be realized (see e.g. Figure S17 for a possible scheme to use in integrating an ELISA-based assay using two valves in parallel connection).

This paper demonstrates electrical valves based on hydrophobic electrotextiles (an electrically conductive textile, presenting an electrically insulating and hydrophobic surface coatings) that can be integrated into 3D paper microfluidic devices. When the valve is "off", a liquid (aqueous solutions) cannot pass through the electrotextile. When an electrical potential is applied between the electrotextile and the liquid, the liquid can penetrate through the textile due to electrowetting. This phenomenon is different from previously demonstrated electrowetting on dielectrics (which works on planar surfaces).[45] These valves have five advantages: i) They can easily be integrated into multi-layer printed microfluidic devices. ii) They are sufficiently fast for applications in microfluidics (they actuate in less than 1 second), and they require little power (100 µW or less) for operation. iii) They have no moving parts. iv) They do not react chemically with the aqueous solutions upon actuation. v) They work with different aqueous solutions including low surface-tension liquids (water with 50% ethanol), solutions containing surfactants, and bioanalytes. Their main disadvantages are: they require high voltages (100-1000 Volts), they are bistable and we cannot control the flow rate, they are effectively irreversible and cannot be closed before the liquid in the channel completely passes through the valve.

We have also demonstrated paper microfluidic circuits with several valves integrated

to form: i) autonomous fluidic timers, ii) logic fluid flow-control without need for an external electronic control logics or processor. We have also shown a small, low-cost and portable electronic device that can deliver high voltages for controlling the valve and that operates with a single AA battery.

Integration of electrotextile valves in paper microfluidics will be especially interesting to explore in applications where timed multistep reactions are required, such as in paper-based ELISA[9,10], electrochemiluminescence (ECL)[13], or nucleic acid biosensors[14]. We believe that electrotextile valves are also suitable for other microfluidic and Lab-on-a-Chip systems that are based on thin materials[55,56], or open-channel paper microfluidics.[57–59] Electrotextiles would be best suited for fabrication by lamination, and thus compatible with processes that fabricate paper and foil devices. Bonding the textile layer between the silicone slabs (such as PDMS) is more cumbersome than lamination with thermoplastics and hot pressing. For silicone devices, the best established approach is channel closure by pinching either by pneumatics[60] or mechanical pins[61]. Elastomer valves are advantageous as they can be quickly opened and closed reversibly, but suffer from more expensive and complicated electromechanical control units than the simple high-voltage power source required for valves presented here.

Experimental Section

Materials: Woven copper (product code: 9224T819) and aluminum (product code: 9224T819) woven textiles were purchased from McMaster-Carr. Plastic textile with a conductive coating (VeilShield™) was purchased from LessEMF Inc. This material was based on polyester threads, which were woven with large spacing and bound together through melting to avoid sliding or separation of threads. This material had conductive electroplated metal (Zn/Ni/Cu) coating. Lens Paper (Whatman 105) was purchased from Sigma-Aldrich (we measured all geometrical parameters of materials using macro photography and a digital

caliper). 2% starch indicator was obtained from VWR. 1M p-toluenosulfonic acid, 0.5M KI and 30mM $Na_2S_2O_3$ were prepared in milli-Q water.

Preparations of different materials for valves: For electrical insulation, all valve materials were coated with Parylene-C (Paratronix Inc., Attleboro, MA). A hydrophobic coating was applied to surfaces using soluble fluoroplastic DuPont™ Teflon® AF (Details of coating procedures are given in supplementary information). We chose Teflon AF because it has a low surface energy (the contact angle of water on Teflon AF $\theta_{H_2O} = 105^{\circ}$).

High voltage power supply: A Keithly 2410 Source-meter or self-built custom low-cost power-supply (Figure S11), were used as a single channel voltage source up to voltages 1.1kV and 0.65kV, respectively. The source meter was controlled manually or through a serial port using MATLAB.

Actuation voltage measurements: To determine the necessary voltage threshold to open the valve, we used an experimental setup (Figure S2), containing: i) a single-use valve; ii) computer-controlled voltage source (Keithly 2410 source meter, with maximum output voltage of 1.1 kV and current 100μA); iii) a digital SLR camera (Canon EOS 550D) with video and audio recording capability equipped with macro lens kit; and iv) a personal computer, which was controlling the voltage source over RS232/USB interface. The single-use valves were prepared by bonding the electrotextile materials to a blotting paper using a thermoplastic (PE) film in a hot-press. We deposited a 20μL droplet of a solution to the valve, and a source electrode wire was then placed into the droplet using a micropositioner (Thorlabs). We then applied a voltage ramp to the valve, while filming the drop, and measured the current as a function of voltage. We continued the measurements until the drop penetrated the valve. A computer program was written in MATLAB 2014 to control the voltage ramping from 0V to 1000V at a rate of 5V/s (total 200s) with 10V steps.

Measurement of liquid contact angles on Teflon AF: We determined the contact angles of different liquids using Si wafers coated with a layer of Parylene-C, and Teflon-AF. We

measured the contact angle of liquids on the Si wafers, as a function of voltage, using the same in-house built goniometry setup as described above (see Figure S2).

Fabrication of paper devices: Paper microfluidic devices were prepared by printing wax patterns, with a Xerox ColorQube wax printer, on Whatman™ Chromatography paper 1. We printed conductors on the paper using carbon ink (Ercon inc.) through stencil masks or manually. The devices were assembled using plastic films (63µm thick polyethylene) as a binder between the sheets. We cut holes in the plastic films for liquid penetration, stacked the plastic films between the papers and the electrotextiles and hot pressed at 210˚C for 1 minute to form a strong adhesion between the layers. The devices were enclosed using the same plastic film to prevent evaporation (see Figure 2).

Characterization of valves at different angles vs. gravity: We fabricated devices by embedding aluminum textile (71µm fiber diameter with a 10µm Parylene C coating and a Teflon-AF coating) between two layers of paper. The paper layers had circular reservoirs (7.5mm diameter), printed using wax printing (a Xerox ColorQube) to confine the liquid and prevent it from sliding of the surface at different angles. We printed carbon ink into the top reservoir as the electrode to the valve. We placed 20µL of an aqueous solutions containing Acid Red into the reservoir and increased the voltage applied between the electrode and the textile until the valve opened and the red dye passed. We varied the angle of the devices from 0˚ (droplet on top of paper) to 180˚ (droplet was hanging on the paper) to analyze the behavior of the valve as a function of gravity.

Preparation and analysis of the Iodate assay: Circular indicator pads (7 mm diameter) were created using wax printing. 10 µL starch indicator was deposited on the pad and dried. We stored the reagents in paper in different sectors (Another 7mm diameter circular input pad was divided into three equal areas using 2 pt line in Illustrator. A narrower line could not stop wicking), due to incompatibility between the reagents. 4 µL of 1M p-toluenosulfonic acid, 2µL of 0.5 M KI, and 4µL of 30 mM $Na_2S_2O_3$ solutions were stored in these three sectors and

dried in an oven at 60 ˚C. We assembled an integrated device, where a preloaded indicator pad and a gate mesh were bonded using the hot pressing, and an input pad was attached using a thermal sealer which allowed to bond surrounding areas without direct heating of the stored reagents.

We tested the assay by depositing 40 µL of sample to the input pad. We used a custom built mechanical shaker shown in Figure S15. After 3 min of shaking, the reagent mixture was transferred to an indicator pad. The colorimetric signal was recorded with a camera (Canon EOS 550D, EF-S 24 mm F2.8 lens), and evaluated using MATLAB, by calculating the relative change in brightness (linear sum of individual RGB channels) of the indicator area.

Supporting Information

Supporting Information is available from the Wiley Online Library or from the author.

Acknowledgements

A. A. and M. M. H contributed equally to this work. We thank Chien-Chung Wang for his help with iodate assay. Christoph Keplinger was helpful in discussion of high voltage instrumentation. Jim MacArthur and The Electronic Instrument Design Lab (Department of Physics, Harvard University) provided an excellent environment for the development of the electronic part of the system. A. A. thanks the Swedish Research Council (VR) for a post-doctoral fellowship. M. M. H. acknowledges support from Marie Curie IOF FP7 for project nanoPAD (Grant Agreement Number 330017), the Bo Rydins stiftelse (SCA AB), and the Sweden-America Foundation. F.G. thanks the German Research Foundation (GU 1468/1-1) for research support. This work was partially funded by NSF award DMR-1420570.

Received: ((will be filled in by the editorial staff))
Revised: ((will be filled in by the editorial staff))
Published online: ((will be filled in by the editorial staff))

References

[1] A. K. Yetisen, M. S. Akram, C. R. Lowe, *Lab Chip* **2013**, *13*, 2210.

[2] D. M. Cate, J. a Adkins, J. Mettakoonpitak, C. S. Henry, **2015**, *87*, 19.

[3] E. W. Nery, L. T. Kubota, *Anal. Bioanal. Chem.* **2013**, *405*, 7573.

[4] J. Adkins, K. Boehle, C. Henry, *Electrophoresis* **2015**, *36*, 1811.

[5] E. J. Maxwell, A. D. Mazzeo, G. M. Whitesides, *MRS Bull.* **2013**, *38*, 309.

[6] J. Hu, S. Wang, L. Wang, F. Li, B. Pingguan-Murphy, T. J. Lu, F. Xu, *Biosens. Bioelectron.* **2014**, *54*, 585.

[7] X. Li, D. R. Ballerini, W. Shen, *Biomicrofluidics* **2012**, *6*, DOI 10.1063/1.3687398.

[8] D. D. Liana, B. Raguse, J. Justin Gooding, E. Chow, *Sensors (Switzerland)* **2012**, *12*, 11505.

[9] S. Ramachandran, E. Fu, B. Lutz, P. Yager, *Analyst* **2014**, *139*, 1456.

[10] A. C. Glavan, D. C. Christodouleas, B. Mosadegh, H. D. Yu, B. S. Smith, J. Lessing, M. T. Fernández-Abedul, G. M. Whitesides, *Anal. Chem.* **2014**, *86*, 11999.

[11] S. Wang, L. Ge, X. Song, J. Yu, S. Ge, J. Huang, F. Zeng, *Biosens. Bioelectron.* **2012**, *31*, 212.

[12] K. N. Han, J.-S. Choi, J. Kwon, V. Gubala, L. F. Harris, A. J. Ricco, M. X. Tan, D. E. Williams, K. N. Han, C. A. Li, G. H. Seong, R. Safavieh, D. Juncker, A. M. Foudeh, Fatanat, T. Didar, T. Veres, M. Tabrizian, G. G. Lewis, J. S. Robbins, S. T. Phillips, A. W. Martinez, S. T. Phillips, G. M. Whitesides, E. Carrilho, J. Hu, X. Wei, B. Ngom, Y. Guo, X. Wang, D. Bi, X. Ge, C. Parolo, A. de la Escosura-Muñiz, A. Merkoçi, B. A. Rohrman, V. Leautaud, E. Molyneux, R. R. Richards-Kortum, L. Ge, A. W. Martinez, S. T. Phillips, G. M. Whitesides, A. C. Glavan, H. Liu, R. M. Crooks, E. Fu, H. Liu, X. Li, R. M. Crooks, Y. K. Oh, H. A.

Joung, S. Kim, M. G. Kim, J. C. Cunningham, N. J. Brenes, R. M. Crooks, E. Robilotti, S. Deresinski, B. A. Pinsky, J. Vinjé, K. F. Lei, Y. K. C. Butt, Y. Li, C. Zhang, D. Xing, V. Costantini, K. Pombubpa, L. Kittigul, H. S. Kim, A. E. Hagström, *Sci. Rep.* **2016**, *6*, 25710.

[13] M. Zhang, L. Ge, S. Ge, M. Yan, J. Yu, J. Huang, S. Liu, *Biosens. Bioelectron.* **2013**, *41*, 544.

[14] J. T. Connelly, J. P. Rolland, G. M. Whitesides, *Anal. Chem.* **2015**, *87*, 7595.

[15] S.-J. Lo, S.-C. Yang, D.-J. Yao, J.-H. Chen, W.-C. Tu, C.-M. Cheng, *Lab Chip* **2013**, *13*, 2686.

[16] Y. Jiang, Z. Hao, Q. He, H. Chen, *RSC Adv.* **2016**, *6*, 2888.

[17] C. K. W. Koo, F. He, S. R. Nugen, *Analyst* **2013**, *138*, 4998.

[18] P. Zwanenburg, X. Li, X. Y. Liu, *Proc. IEEE Int. Conf. Micro Electro Mech. Syst.* **2013**, 253.

[19] M. M. Hamedi, V. E. Campbell, P. Rothemund, F. Güder, D. C. Christodouleas, J.-F. Bloch, G. M. Whitesides, *Adv. Funct. Mater.* **2016**, n/a.

[20] A. W. Martinez, S. T. Phillips, Z. Nie, C.-M. Cheng, E. Carrilho, B. J. Wiley, G. M. Whitesides, *Lab Chip* **2010**, *10*, 2499.

[21] S. Jahanshahi-Anbuhi, P. Chavan, C. Sicard, V. Leung, S. M. Z. Hossain, R. Pelton, J. D. Brennan, C. D. M. Filipe, *Lab Chip* **2012**, *12*, 5079.

[22] X. Y. Liu, C. M. Cheng, A. W. Martinez, K. A. Mirica, X. J. Li, S. T. Phillips, M. Mascareñas, G. M. Whitesides, in *IEEE MEMS*, **2011**, pp. 75–78.

[23] H. Chen, J. Cogswell, C. Anagnostopoulos, M. Faghri, *Lab Chip* **2012**, *12*, 2909.

[24] F. He, J. Grimes, S. D. Alcaine, S. R. Nugen, *Analyst* **2014**, *139*, 3002.

[25] T. Guo, T. Meng, W. Li, J. Qin, Z. Tong, Q. Zhang, X. Li, *Nanotechnology* **2014**, *25*, 125301.

[26] L. Cai, M. Zhong, H. Li, C. Xu, B. Yuan, *Biomicrofluidics* **2015**, *9*, 46503.

[27] R. Gerbers, W. Foellscher, H. Chen, C. Anagnostopoulos, M. Faghri, *Lab Chip* **2014**, *14*, 4042.

[28] S. Jahanshahi-Anbuhi, A. Henry, V. Leung, C. Sicard, K. Pennings, R. Pelton, J. D. Brennan, C. D. M. Filipe, *Lab Chip* **2013**, *14*, 229.

[29] B. Lutz, T. Liang, E. Fu, S. Ramachandran, P. Kauffman, P. Yager, *Lab Chip* **2013**, *13*, 2840.

[30] B. J. Toley, J. A. Wang, M. Gupta, J. R. Buser, L. K. Lafleur, B. R. Lutz, E. Fu, P. Yager, *Lab Chip* **2015**, *15*, 1432.

[31] C. C. Wang, J. W. Hennek, A. Ainla, A. A. Kumar, W. J. Lan, J. Im, B. S. Smith, M. Zhao, G. M. Whitesides, *Anal. Chem.* **2016**, *88*, 6326.

[32] J. Ding, B. Li, L. Chen, W. Qin, *Angew. Chemie - Int. Ed.* **2016**, *55*, 13033.

[33] B. Lu, S. Zheng, B. Q. Quach, Y.-C. Tai, *Lab Chip* **2010**, *10*, 1826.

[34] J. B. Fortin, T.-M. Lu, *J. Vac. Sci. Technol. A Vacuum, Surfaces, Film.* **2000**, *18*, 2459.

[35] DuPont™, *Amorphous Polymer Resis Teflon ® AF - Datasheet*, **n.d.**

[36] A. A. Mariod, H. F. Adam, *Acta Sci. Pol. Technol. Aliment.* **2013**, *12*, 135.

[37] D. Chatterjee, B. Hetayothin, A. R. Wheeler, D. J. King, R. L. Garrell, *Lab Chip* **2006**, *6*, 199.

[38] S. K. Cho, H. Moon, C. J. Kim, *J. Microelectromechanical Syst.* **2003**, *12*, 70.

[39] S. Urazhdin, N. O. Birge, W. P. Pratt, J. Bass, *Phys. Rev. Lett.* **2003**, *91*, 146803.

[40] H. Moon, S. K. Cho, R. L. Garrell, C. J. Kim, *J. Appl. Phys.* **2002**, *92*, 4080.

[41] F. Mugele, J.-C. Baret, *J. Phys. Condens. Matter* **2005**, *17*, R705.

[42] P. Paik, V. K. Pamula, M. G. Pollack, R. B. Fair, *Lab Chip* **2003**, *3*, 28.

[43] M. G. Pollack, a D. Shenderov, R. B. Fair, *Lab Chip* **2002**, *2*, 96.

[44] A. R. Wheeler, H. Moon, C. a. Bird, R. R. O. Loo, C. J. Kim, J. a. Loo, R. L. Garrell, *Anal. Chem.* **2005**, *77*, 534.

[45] A. R. Wheeler, *Science* **2008**, *322*, 539.

[46] K. H. Kang, *Langmuir* **2002**, *18*, 10318.

[47] V. Peykov, A. Quinn, J. Ralston, *Colloid Polym. Sci.* **2000**, *278*, 789.

[48] M. Vallet, M. Vallade, B. Berge, *Eur. Phys. J. B* **1999**, *11*, 583.

[49] E. W. Washburn, *Proc. Natl. Acad. Sci. U. S. A.* **1921**, 115.

[50] M. M. Hamedi, A. Ainla, F. Güder, D. C. Christodouleas, M. T. Fernández-Abedul, G. M. Whitesides, *Adv. Mater.* **2016**, 5054.

[51] E. Carrilho, A. W. Martinez, G. M. Whitesides, *Anal. Chem.* **2009**, *81*, 7091.

[52] F. Güder, A. Ainla, J. Redston, B. Mosadegh, A. Glavan, T. J. Martin, G. M. Whitesides, *Angew. Chemie Int. Ed.* **2016**, *2138*, n/a.

[53] A. Nemiroski, D. C. Christodouleas, J. W. Hennek, A. A. Kumar, E. J. Maxwell, M. T. Fernández-Abedul, G. M. Whitesides, *Proc. Natl. Acad. Sci. U. S. A.* **2014**, *111*, 11984.

[54] N. M. Myers, E. N. Kernisan, M. Lieberman, *Anal. Chem.* **2015**, *87*, 3764.

[55] M. Focke, D. Kosse, C. Müller, H. Reinecke, R. Zengerle, F. von Stetten, *Lab Chip* **2010**, *10*, 1365.

[56] S. Lutz, P. Weber, M. Focke, B. Faltin, J. Hoffmann, C. Müller, D. Mark, G. Roth, P. Munday, N. Armes, O. Piepenburg, R. Zengerle, F. von Stetten, *Lab Chip* **2010**, *10*, 887.

[57] M. M. Thuo, R. V. Martinez, W. J. Lan, X. Liu, J. Barber, M. B. J. Atkinson, D. Bandarage, J. F. Bloch, G. M. Whitesides, *Chem. Mater.* **2014**, *26*, 4230.

[58] A. C. Glavan, R. V Martinez, E. J. Maxwell, A. B. Subramaniam, R. M. D. Nunes, S. Soh, G. M. Whitesides, *Lab Chip* **2013**, *13*, 2922.

[59] C. Renault, X. Li, S. E. Fosdick, R. M. Crooks, **2013**, DOI 10.1021/ac401786h.

[60] M. A. Unger, H. Chou, T. Thorsen, A. Scherer, S. R. Quake, *Science (80-.).* **2000**, *288*, 113.

[61] B. Mosadegh, A. D. Mazzeo, R. F. Shepherd, S. a Morin, U. Gupta, I. Z. Sani, D. Lai, S. Takayama, G. M. Whitesides, *Lab Chip* **2014**, *14*, 189.

ALL DISPLAY ITEMS ARE INTENDED TO BE SINGLE COLUMN (300DPI RESOLUTION)

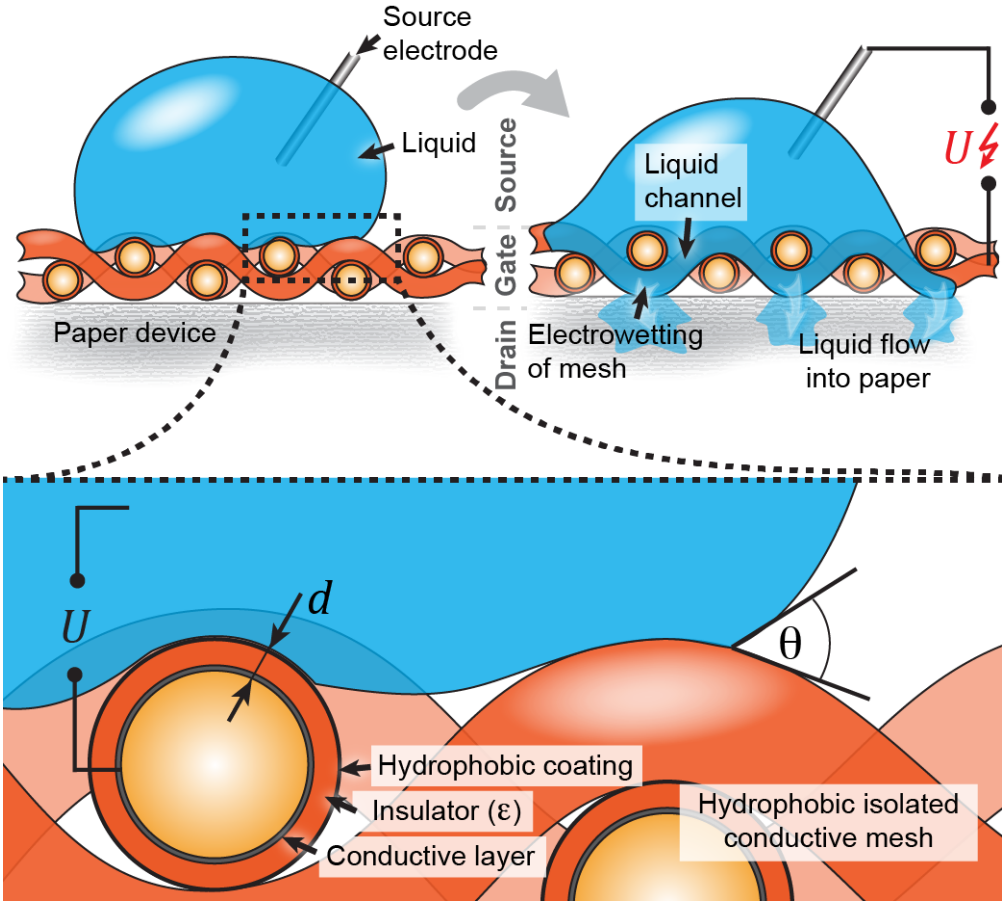

Figure 1. *Principle of the bistable electrical valve.* Schematic diagram of the operation of the valve, which is based on the principles of electrowetting on dielectric (EWOD). The gate electrode is a conductive textile covered with layers of insulator and hydrophobic coating ("electrotextile"). This electrotextile is not permeable to liquid. The application of a voltage between the liquid and the electrotextile allows liquid to flow into the paper layer underneath due to electrowetting.

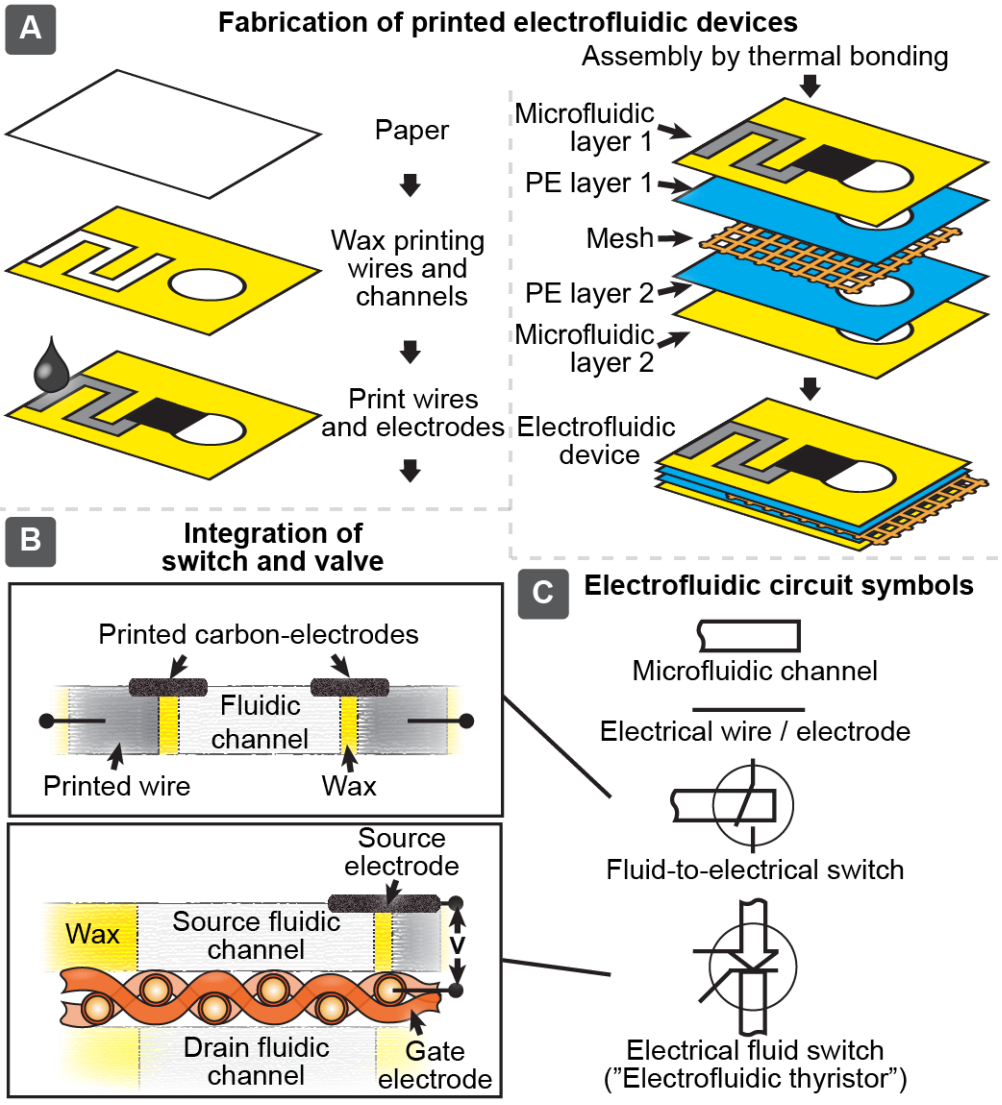

Figure 2. *Design and fabrication of printed electrofluidic devices.* (A) Schematic diagram of the fabrication of three-dimensional printed electrofluidic circuits. Microfluidic channels are printed using wax printing, followed by printing of electrodes (for valves and switches) and electrical wires on the paper layers. Conductive, insulated, and hydrophobic "electrotextiles" are then bonded with the paper layers using hot-lamination with polyethylene films. (B) Schematic cross-section of a fluid-to-electrical switch, and Schematic cross-section of an integrated valve, containing two microfluidic layers, and a valve layer. The valve is actuated when a voltage is applied between the liquid ("source electrode") and the electrotextile ("gate electrode") whereupon liquid can pass from the "liquid source" into the "liquid drain". (C) Circuit diagram symbols for printed microfluidic channels, printed wires/electrodes, integrated fluid-electrical switches, and valves ("electrofluidic thyristors").

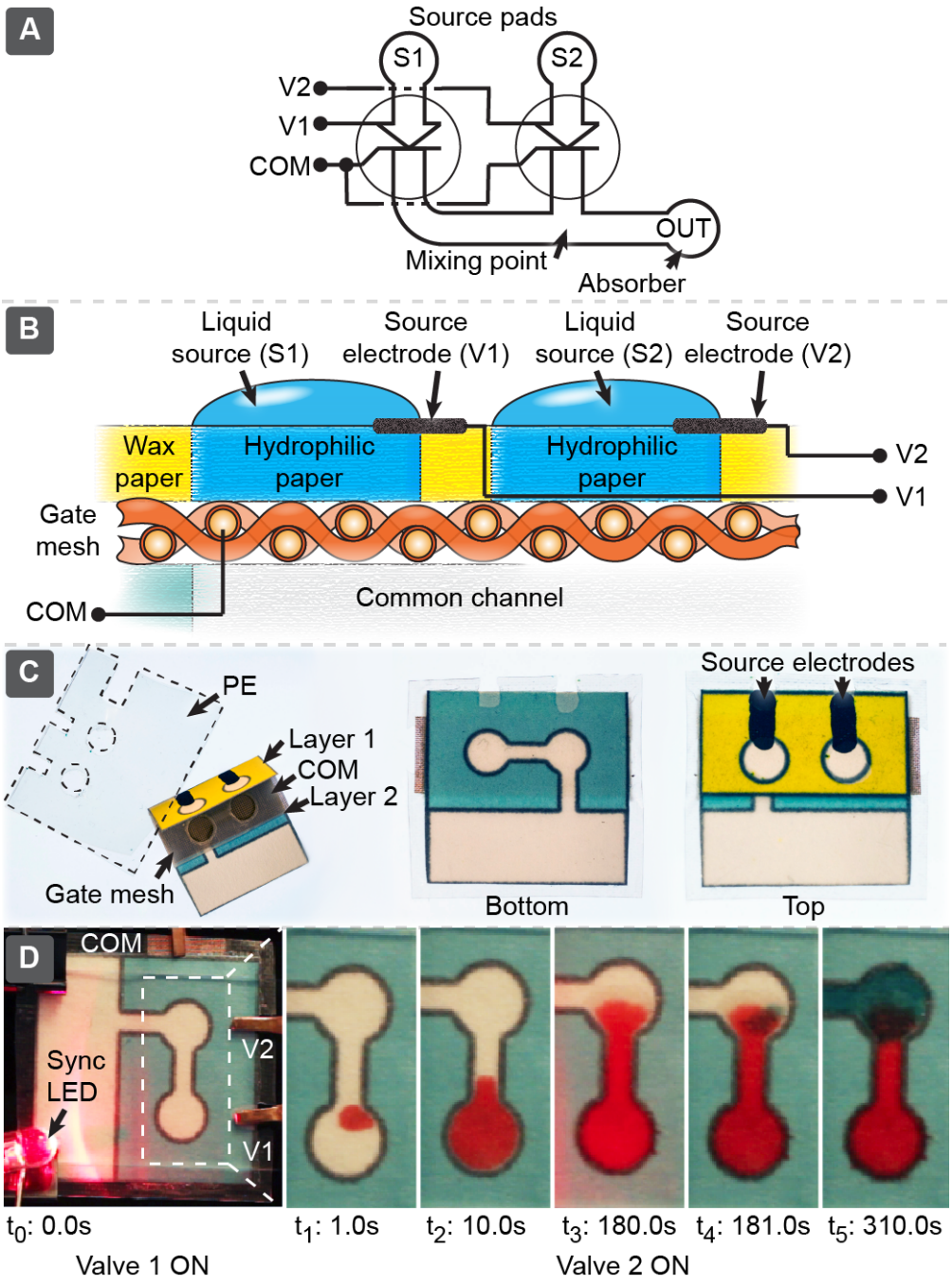

Figure 3. *Valves in parallel connection*. (A) Circuit diagram of two individually addressable electrofluidic valves connected to a common drain channel. (B) Schematic cross-section of the device. (C) Photos of the fabrication process. The devices were printed on a single sheet of paper, which was folded around the electrotextile and laminated using polyethylene films. (D) Photographs of the operation of the device where two aqueous solutions in separate reservoirs (red and green) are injected into a common channel. An LED indicates when an electrical pulse is applied to open each valve.

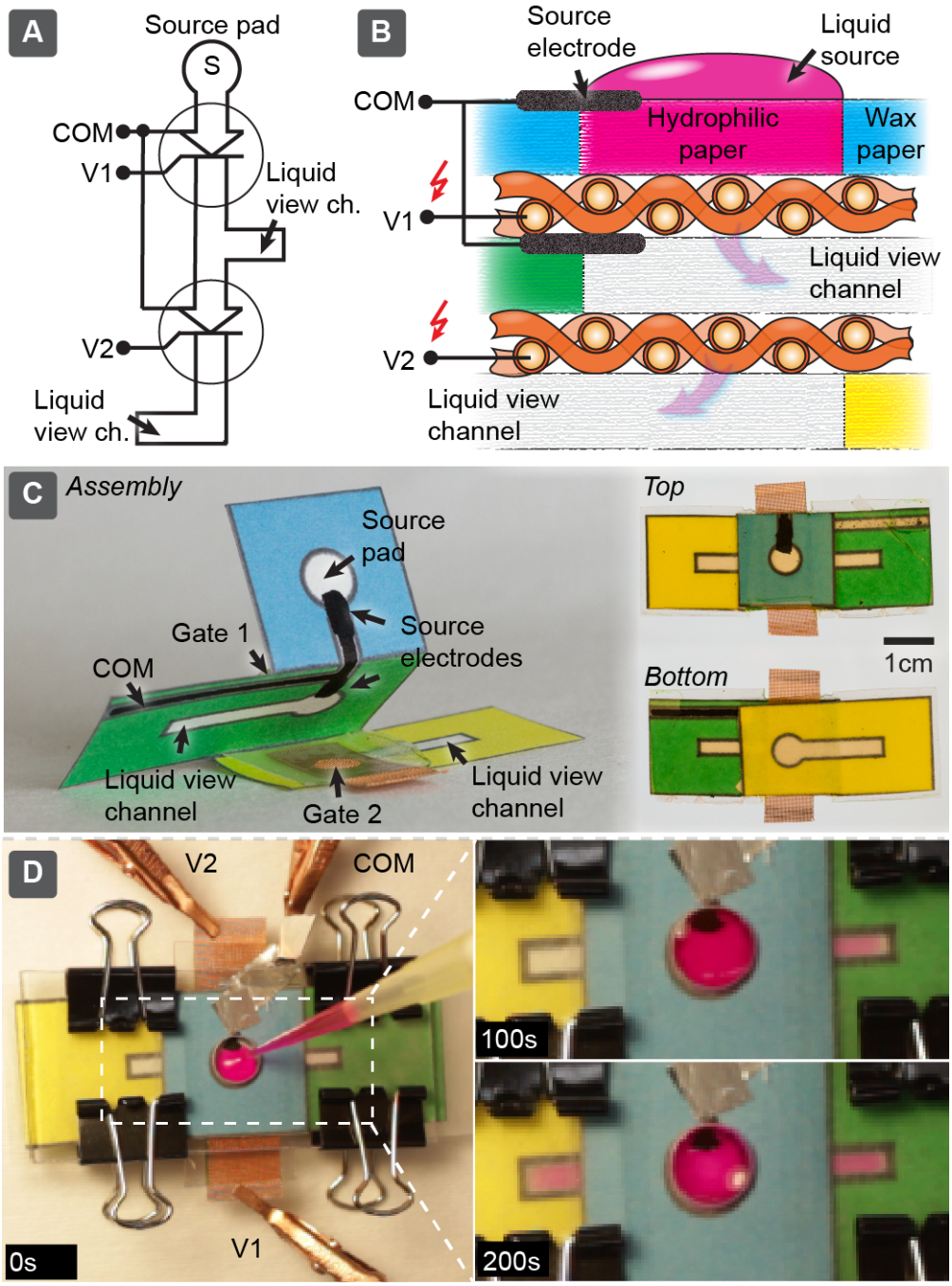

Figure 4. *Valves in serial connection.* (A) Circuit diagram of two individually addressable electrofluidic valves connected in series. We have used liquid view channels to visualize the presence of liquid in the middle layer, which would otherwise not be visible due to the stacked structure (B) Schematic cross-section of the device containing three microfluidic layers separated by two layers. (C) Photographs of the device fabrication where we printed the

microfluidic channels on a single sheet of paper, folded the paper around the electrotextile and laminated the device with PE films. (D) Time-lapse photographs showing the operation of the device, where the liquid passes the first valve (by applying a voltage V1), and thereafter the second valve (by applying a voltage V2).

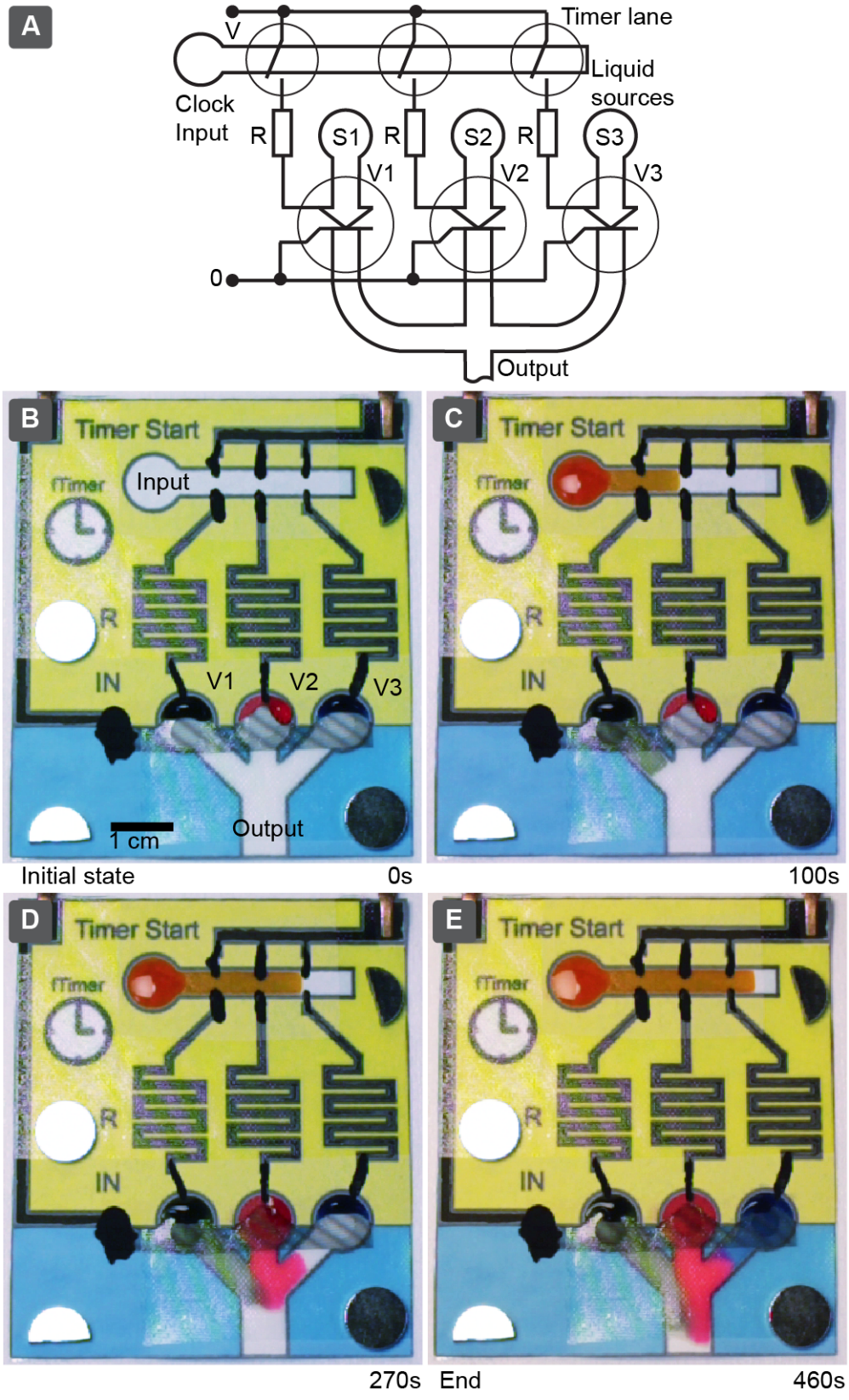

Figure 5. *Electrofluidic timer*. (A) Circuit diagram of a fluidic timer. (B) Photograph of a fluidic timer device. (C-E) Time-lapse photographs of the device. where the liquid propagation (orange liquid) in the timer channel trigger sequential addition of three colored

liquids (black, red, blue) from three reservoirs into a common output, by opening a valve for each liquid (V1, V2, V3).

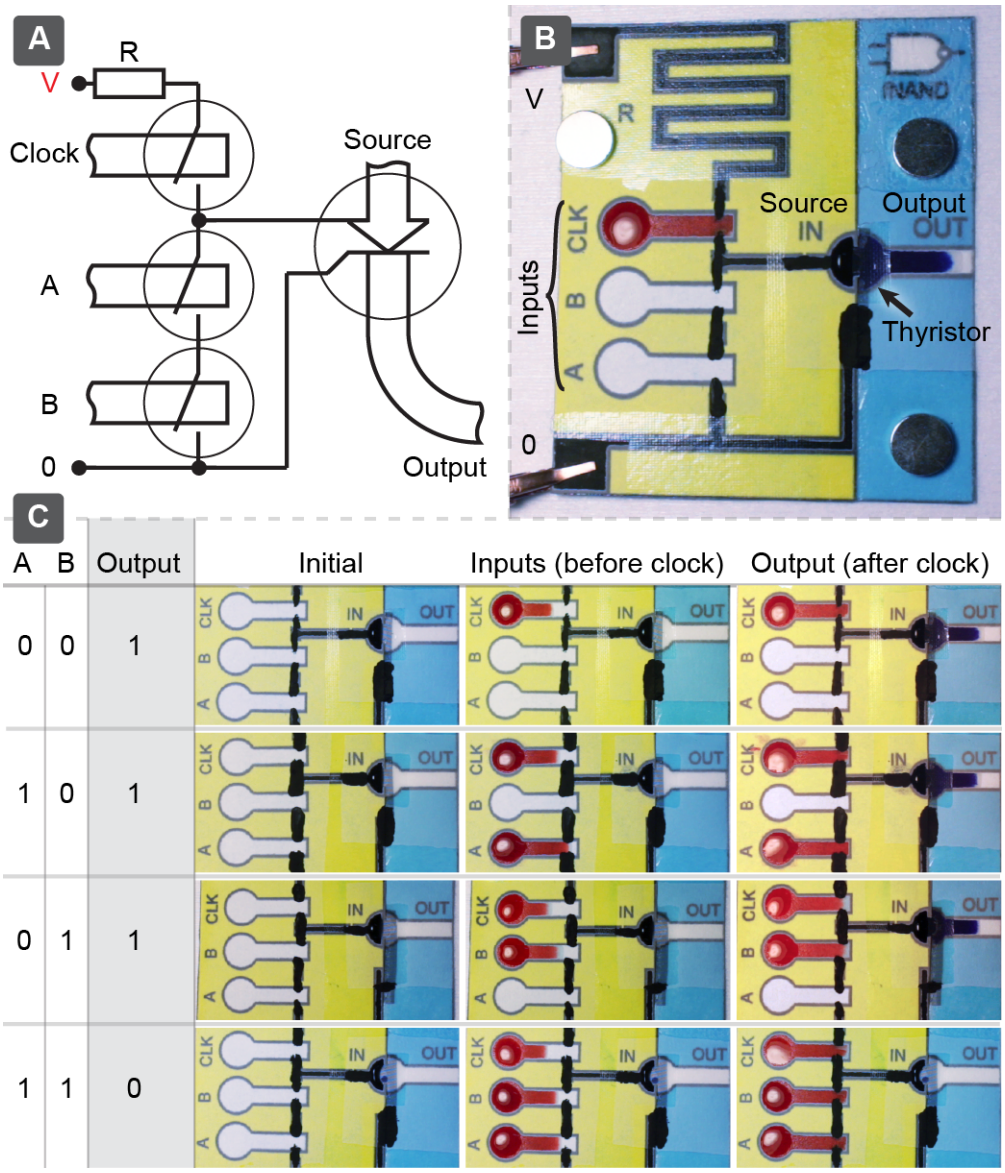

Figure 6. *Electrofluidic NAND gate (fNAND).* (A) Circuit diagram of a fluidic NAND, and (B) Photograph of a synchronous fluidic NAND gate. The logical state (1) is represented by the present of a liquid in the inputs (A and B) or output (OUT), and the lack of a liquids represents the logical state (0). The device is triggered by addition of a liquid to the clock

input (CLK) (C) Photographs of all four logical states of the device. The input liquids are red, and the output liquid is blue.

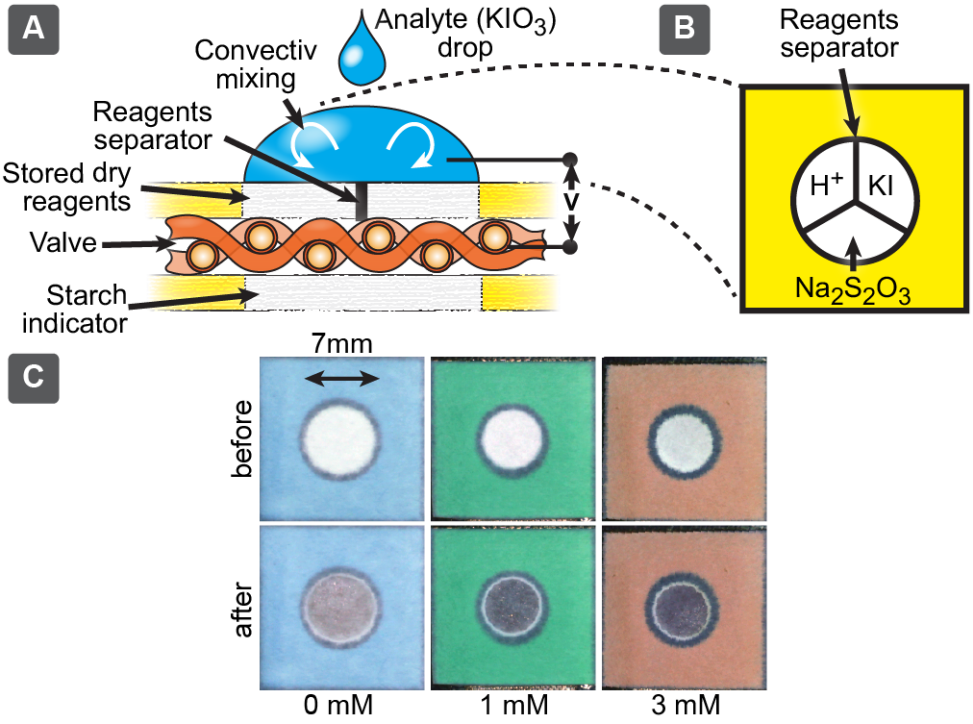

Figure 7. (A) Schematic diagram of the integrated iodate assay device. To operate the device, we first add the analyte (KIO_3) to the input pad (B) composed of three separated areas, that each store the individual components H^+, KI, and $Na_2S_2O_3$. The analyte volume is sufficiently large to allow convective mixing of the components upon mechanical shaking. After mixing (3 minutes) we open the valve and the product is transferred to the starch indicator pad. (C) Photographs of the device showing colorimetric signal depending on the analyte concentration.

Table 1. Properties of the three woven materials for electrowetting.

Property	**Copper textile**	**Aluminum textile**	**Polyester textile** Metal plated
Electrical conductivity	Intrinsic	Intrinsic	Zn/Ni/Cu plating
Insulation layer		~10μm Parylene-C	
Hydrophobic layer		Dip-coated with Teflon AF 2400	
Resistivity (Ohm/sq.)	~10^{-8}	~10^{-8}	0.1
Fiber diameter (μm)	136	71	22
Mesh opening size (μm)	143	62	157
Mesh period (μm)	279	136	179
Thickness (μm)	300	180	60
Liquid breakthrough pressure (mbar)	10.1 (*σ=3.4*)	18.8 (*σ=4.1*)	6.1 (*σ=2.0*)
Cost (USD/cm^2)	0.018	0.03	0.0042

Table 2. Measured actuation voltage for an aluminum textile (according to table 1) for different solutions.

Solution	Surface tension (mN/m)	Actuation voltage (standard deviation, n=7)
Water	72	450 (320)
5% EtOH in Water	56	300 (210)
10% EtOH in Water	48	141 (75)
50% EtOH in Water	29	80 (21)
EtOH	22	-
1mM Pluronic F68 in PBS		188 (45)
BSA (50g/L) in PBS		480 (330)
Blood		240 (63)

The table of contents entry

Textile valves based on electrowetting principle and their use in paper microfluidics are presented. These valves can be integrated into paper microfluidics monolithically, they require no mechanically moving parts, they are fast, low-energy and work with variety of aqueous solutions. Furthermore, such valves can be combined into self-regulating autonomous circuits and used for reagent addition in assays.

Keyword

A. Ainla, M. M. Hamedi, F. Güder, G. M. Whitesides*

Electrical Textile Valves for Paper Microfluidics

ToC figure (size: 55 mm broad × 50 mm)

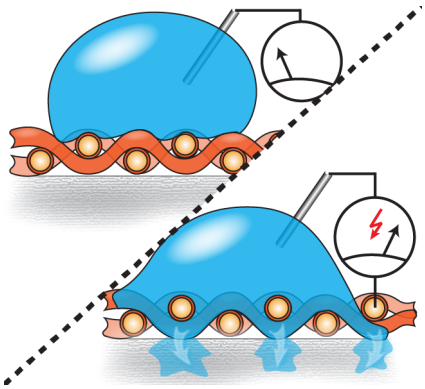

Supporting Information

Electrical Textile Valves for Paper Microfluidics

*Alar Ainla, Mahiar M. Hamedi, Firat Güder and George M. Whitesides**

Currently existing valve technologies for paper devices

Table S1. Summary of flow-control and valve technologies relevant for paper microfluidic devices. The table includes currently reported paper valves, as well as other methods to regulate flows in paper microfludics, and valves which have been reported for other types of microfluidics, but could be relevant also in the context of paper devices. We divide devices by their type into chemical (Chem.) and physical (Phys.), where chemical devices operate based on changes in chemical composition (reaction or dissolution), while physical devices do not involve such changes. Physical devices are less likely to interfere with assays, since no additional compounds are released during the actuation of these valves.

Reference	General description	Actuated by/ Normal state/ Operation mode	Type	Flow control is used during / repeatability	*Pros*	*Cons*
Valves for wicking-based paper microfluidic devices						
Y. Jiang, Z. Hao, Q. He and H. Chen, *RSC Adv.*, 2016, **6**, 2888–2894.	Liquid impermeable hydrophobic barrier is treated with hand-held corona generator, which renders it hydrophilic and liquid permeable (opening is fast, within 1s).	Electric plasma / Closed / Discrete opening	Chem	Operation / One time	Simple low-cost paper device. No moving parts. Electrical control. Fast to open (in 1s).	Corona generator is expensive (>500USD). Electromagnetic noise (10-45kV, 4.5MHZ). Safety concerns. Large energy consumption (40W). Plasma may damage sample.

C. K. W. Koo, F. He and S. R. Nugen, *Analyst*, 2013, **138**, 4998–5004.	Electrchemical valves containing printed conductive paper (reactive silver ink), which is treated with hydrophobic thiol. This barrier is not wicked by liquid readily (though not completely impermeable), but when low voltage (4V or above) is applied, it erodes the thiol and wicking speed increases (about 10x).	Electrical signal / Closed / Wicking speed modulation	Chem	Operation / On time	Simple low-cost device. No moving parts. Simple low-voltage electrical control.	Electrochemical reaction may damage sample/reagents. Relatively slow (100s). No complete closure.
P. Zwanenburg, X. Li and X. Y. Liu, *Proc. IEEE Int. Conf. Micro Electro Mech. Syst.*, 2013, 253–256.	Magnetic valve based on paper cantilever containing magnetic PDMS. This cantilever can move and can connect or disconnect the paper channel. Cantilever is moved by an electromagnet .	Electro-magnet / Either Closed or Open / Discrete switching	Phys	Operation / Reversible	Fast switching. Electrical control. Reversible. No chemical interference.	Mechanically moving parts and complicated device design. Electromagnets are quite large.
M. M. Hamedi, V. E. Campbell, P. Rothemund, F. Güder, D. C. Christodoulou, J.-F. Bloch and G. M. Whitesides, *Adv. Funct. Mater.*, 2016, n/a–n/a.	Electrically activated paper actuator, which bends. This cantilever can be used to connect and disconnect paper channel to and from the liquid. Principle of the actuator is based on reversible expansion and contraction of cellulose, when adsorbing water from air. Adsorption is further controlled by electrical heating with PEDOT:PSS heaters made into same paper device.	Electrical heating / Either Closed or Open / Discrete switching	Phys	Operation / Reversible	Low-cost device. Reversible. Simple electrical control.	Mechanically moving parts. High voltage (100V) / power required to heat. Relatively slow 15-20s. High temperature may affect the assay. Actuation depends on the surrounding humidity.
Y. Matsuda, S. Shibayama, K. Uete, H. Yamaguchi and T. Niimi, *Anal. Chem.*, 2015, 1–8.	Electrical heater is used to evaporate liquid, which effectively stops the wicking of liquid front. Heater is printed to the paper using low-resistance silver nanoparticle ink. Valve operates in the range of 10s.	Heat / Open / Stops wicking	Phys	Operation / Repeatable	Simple low-cost paper device. No moving parts. Simple electrical control (5V). Fast and repeatable.	To keep valve closed requires constant power (1.5A, 7.5W). Evaporation changes liquid concentration. High temperature (>60˚C) may damage the sample and alter reactions.
L. Cai, M. Zhong, H. Li, C. Xu and B. Yuan, *Biomicrofluidics*, 2015, **9**, 046503.	Printed surfactant, which solubility depends steeply on temperature, is used to assist the liquid to cross the hydrophobic barrier. Wicking rate depends almost linearly on temperature, complete closure at <15˚C.	Temperature / Either Open or Closed / Wicking speed modulation	Chem	Operation / One time	Simple low-cost paper device. No moving parts. Electrical control possible with heater/cooler. Adjustable flow rate.	Complete closure requires active cooling (15˚C). High temperature (80˚C) may affect chemistry or destroy sample. Surfactant may interfere with the assay.
A. W. Martinez, S. T. Phillips, Z. Nie, C.-M. Cheng,	Push-button ‘on’ valves, which are formed in multilayer paper device, where there is a cavity left between different paper	Mechanical pressing by user / Closed / Discrete opening	Phys	Operation / On time	Simple low-cost paper device. No chemical interference.	Mechanically moving parts. Automation would require more complex actuators

E. Carrilho, B. J. Wiley and G. M. Whitesides, *Lab Chip*, 2010, **10**, 2499–504.	layers, which liquid cannot cross. Once pressed, cavity collapses and liquid connection between the paper layers is formed.					
S. Jahanshahi-Anbuhi, P. Chavan, C. Sicard, V. Leung, S. M. Z. Hossain, R. Pelton, J. D. Brennan and C. D. M. Filipe, *Lab Chip*, 2012, **12**, 5079–5085.	Flap valve, in which a paper cantilever is connecting or disconnecting the channel	Mechanical motion by user / Either Closed or Open / Discrete switching	Phys	Operation / Reversible	Fast switching, Reversible. No chemical interference.	Mechanically moving parts.
X. Y. Liu, C. M. Cheng, A. W. Martinez, K. A. Mirica, X. J. Li, S. T. Phillips, M. Mascareñas and G. M. Whitesides, in *IEEE MEMS*, 2011, pp. 75–78.	Sliding strip, which is moving between two stationary paper layers and can reconfigure the fluidic pathways between them. It allows to switch the sample between different liquid sources, operating as "selector switch".	Mechanical motion by user / Various states. Selector switch / Discrete switching	Phys	Operation / Reversible	Versatile to reconfigure the circuitry of flow paths. No chemical interference.	Mechanically moving parts. Automation would require more complex actuators.
X. Li, X. Li, J. Tian, J. Tian, T. Nguyen, T. Nguyen, W. Shen and W. Shen, *Lab Chip*, 2008, **80**, 9131–9134.	Simple sliding and cantilever valves, made by mechanical cutting assembly of hydrophilic/hydrophobic paper.	Mechanical motion by user / Either Closed or Open / Discrete switching	Phys	Operation / Reversible	Simple low-cost paper device. Reversible actuation. No chemical interference.	Mechanically moving parts. Automation would require more complex actuators.
B. J. Toley, J. A. Wang, M. Gupta, J. R. Buser, L. K. Lafleur, B. R. Lutz, E. Fu and P. Yager, *Lab Chip*, 2015, **15**, 1432–1444.	Liquid triggered expanding actuators (cellulose sponges) are used to mechanically move paper cantilevers and connect, disconnect or divert fluid flow paths. Actuation requires 30µL of fluid.	Liquid / Open or Closed / Discrete switching of flow path	Phys	Operation / One time	No chemical interference. Number of different functions. All regulation on chip. No external control required. Self-regulating liquid networks.	Mechanically moving parts. Complex device structure. Relatively slow (5-50s). No external control possible.
H. Chen, J. Cogswell, C. Anagnostopoulos and M. Faghri, *Lab Chip*, 2012, **12**, 2909.	Lateral flow fluidic diode, which uses deposited surfactant to cross the hydrophobic barrier. Liquid can initially pass only, when it arrives to the diode from surfactant side. Valve, once opened, conducts in both ways.	Liquid / Closed / Discrete opening	Chem	Operation / One time	Simple low-cost paper device. No moving parts. Self-regulating. No external control required.	Actuation program is set during manufacturing. Surfactant may interfere with assay.

R. Gerbers, W. Foellscher, H. Chen, C. Anagnostopoulos and M. Faghri, *Lab Chip*, 2014, **14**, 4042–9.	Vertical flow fluidic diode (similar to previous). Two layers (one hydrophobic and another one containing dried surfactant) are stacked. Valve is opened, when liquid is wicking from the surfactant side, which allows it to pass the hydrophobic barrier. Valve, once opened, conducts in both ways.	Liquid / Closed / Discrete opening	Chem	Operation / One time	Simple low-cost paper device. No moving parts. Self-regulating. No external control required.	Actuation program is set during manufacturing. Surfactant may interfere with assay.
B. R. Lutz, P. Trinh, C. Ball, E. Fu and P. Yager, *Lab Chip*, 2011, **11**, 4274.	Valve based on the competing flows from a limited liquid source, which leads to the disconnection and delayed shut-off.	Liquid / Open / Discrete closure	Phys	Fabrication / One time	No external control required. No chemical interference.	Relatively complex setting to form competing wicking, which combines bulk liquid source and paper device.
Passive flow-control methods for wicking-based paper microfluidic devices						
B. Lutz, T. Liang, E. Fu, S. Ramachandran, P. Kauffman and P. Yager, *Lab Chip*, 2013, **13**, 2840–7.	Dried sugar is used in the paper, which alters the liquid viscosity and wicking time	Liquid / N/A / Wicking speed modulation	Chem	Fabrication / One time	Simple low-cost paper device. No external control required.	Wicking properties are set during manufacturing (sugar deposition). Dissolved sugar may interfere with assay.
I. Jang and S. Song, *Lab Chip*, 2015, **15**, 3405–12.	Flow control based on wax printing method. Printing small amount of wax into the channels allows reducing the flow rate controllably.	Wax amount / N/A / Wicking speed modulation	Phys	Fabrication / N/A	Simple low-cost paper device. No moving parts.	Flow properties are set during manufacturing.
C.-H. Weng, M.-Y. Chen, C.-H. Shen and R.-J. Yang, *Biomicrofluidics*, 2014, **8**, 066502.	Wax printed valves. Thin wax print between the paper layers is liquid permeable, but once heated to 150˚C for 30min the wax wicks into the paper and makes it liquid impermeable (valve is closed)	Temperature / Open / Discrete closure	Phys	Before operation / N/A	Simple low-cost paper device. No moving parts.	Valve state has to be set by heating step before the operation. High temperature may damage reagents stored in the device.
J. H. Shin, J. Park, S. H. Kim and J. K. Park, *Biomicrofluidics*, 2014, **8**.	When porous mesh, like paper is mechanically treated by high-pressure press, material is compressed, which reduces the pore size, and increases the fluidic resistance, reducing the wicking speed. Wicking speed was reduced up to 740% by pressing (max 300bar)	Mechanical pressure / Open / Wicking speed modulation	Phys	Before operation / N/A	Simple low-cost paper device. No moving parts during operation. No chemical interference. Adjustable flow rate.	Requires high-pressure press to adjust the valve (300bar). Valve is normally set before operation. No complete closure possible.
D. L. Giokas, G. Z. Tsogas and A. G. Vlessidis, *Anal. Chem.*, 2014, **86**,	They use razor cuts in the paper channels to modulate the flow rates. Longitudinal channels increase the flow rate, while perpendicular ones decrease	Mechanical cut / N/A / Wicking speed modulation	Phys	Fabrication / N/A	Simple low-cost device. No moving parts. Extends the range of flow rates possible. No chemical interference.	Flow properties are set during the manufacturing.

6202–6207.						
B. J. Toley, B. McKenzie, T. Liang, J. R. Buser, P. Yager and E. Fu, *Anal. Chem.*, 2013, **85**, 11545–52.	Absorber pads (shunts) are placed on the lateral-flow paper channel in order to delay the wicking front. It gives a fixed delay, after which the wicking continues at the same rate. Though not shown, it can be imagined that shunt is actively connected/disconnected also during the operation.	N/A / N/A / Wicking delay	Phys	Fabrication / N/A	Simple low-cost device. No moving parts. Delays wicking, but does not slow down the later flow, as longer channel would do. No chemical interference. Adjustable delay time by shunt geometry.	Extra sample required for filling the shunt. Pre-defined delay. No external control.
S. Jahanshahi-Anbuhi, A. Henry, V. Leung, C. Sicard, K. Pennings, R. Pelton, J. D. Brennan and C. D. M. Filipe, *Lab Chip*, 2013, **14**, 229–236.	Water-soluble Pullulan films, have been placed over small gap in the paper channel. Initially liquid passes the gap, but when Pullulan dissolves, liquid becomes substantially more viscose and flow slowes/stops. This provides delayed shut-off of the flow.	Liquid / Open / Wicking speed modulation	Chem	Fabrication / One time	Simple low-cost device. No moving parts. No external control required, Adjustable flow rate and shut-off by the film geometry	Actuation program is set during manufacturing. Dissolved polymer may interfere with the assay. Actuation may depend on parameters such as room temperature. No complete closure.
Other paper microfluidic devices with flow control						
H. Ko, J. Lee, Y. Kim, B. Lee, C.-H. Jung, J.-H. Choi, O.-S. Kwon and K. Shin, *Adv. Mater.*, 2014, **26**, 2335–40.	Traditional type of electro-wetting to move droplet, on the surface, but the device substrate is paper. Electrodes are printed with carbon ink and coated with parylene and fluorocarbon oil.	Electrical signal / N/A / Droplet motion	Phys	Operation / Reversible	Printed. Fast actuation. Flexible substrate.	Relatively complex fabrication. Not compatible with wicking-based paper microfluidics.
Flow control technologies, which could be relevant for paper microfluidic applications						
G. Londe, A. Chunder, A. Wesser, L. Zhai and H. J. Cho, *Sensors Actuators, B Chem.*, 2008, **132**, 431–438.	PNIPAAm and silica nanoparticles based surface treatment, which hydrophobic/hydrophilic state is switched by temperature. Above 65˚C it is hydrophobic and below that hydrophilic. This device is shown in glass microfluidics, but principle would be compatible with paper devices as well.	Temperature / Closed / Discrete opening	Phys	Operation / One time	No moving parts. Simple electrical control by heating.	More complex fabrication. High temperature may damage sample or reagent and require higher heating power.
M. Xiong, B. Gu, J. D. Zhang, J. J. Xu, H. Y. Chen and H. Zhong, *Biosens. Bioelectron.*, 2013, **50**, 229–234.	Photopatterned PNIPAAm film is used to modulate surface wettability and reversibly release and adsorb GOx to switch on and off the enzymatic reaction.	Temperature / N/A / Chemical switch	Chem	Operation / Reversible	Simple low-cost device. No moving parts. External control can be achieved by heating and cooling. Actuation temperature is mild.	Temperature may affect other aspects of chemistry. Since actuation temperature is about 35˚C, switching may require active cooling.
G. Chen, F. Svec and D. R. Knapp,	PNIPAAm based microvalve, which is actuated by high power	Light induced temperature change /	Phys	Operation / Reversible	No moving parts. Simple electrical control by light.	High temperature may damage sample or reagent

Lab Chip, 2008, **8**, 1198–204.	light, that causes heating. Valve opens and closes in few seconds	Closed / Discrete opening			Reversible actuation.	and require higher heating power (light source).
T. Guo, T. Meng, W. Li, J. Qin, Z. Tong, Q. Zhang and X. Li, *Nanotechnology*, 2014, **25**, 125301.	Microchannel coated with a layer of silanized TiO_2-SiO_2 nanoparticles. This layer is normally hydrophobic and repels the liquid, but becomes hydrophilic when exposed to UV light, which degrades the organic layer from its surface. Hydrophobicity recovers in 2weeks. This is not paper device, but idea could be compatible.	UV light / Closed / Wicking speed modulation	Chem	Before operation / Reversible (but slow)	Simple low-cost device. No moving parts.	Long switching time and high doze of UV (12W, 254nm for 6h). Shown only as pre-operation modification.
F. He, J. Grimes, S. D. Alcaine and S. R. Nugen, *Analyst*, 2014, **139**, 3002–8.	They use silver electrode, which has surface assembled monolayer of hydrophobic fluorinated thiol. Liquid normally does not cross the electrode, until voltage in the range of 2-4V is applied, which erodes the coating and wets the electrode. This is not a paper device, but elastic channel made in PET film.	Electrical signal / Closed / Discrete opening	Chem	Operation / One time	Simple low-cost device. No moving parts. Simple low-voltage electrical control.	Electrochemical reaction may damage sample/reagents. Relatively slow (10-40s).
B. Mosadegh, A. D. Mazzeo, R. F. Shepherd, S. a Morin, U. Gupta, I. Z. Sani, D. Lai, S. Takayama and G. M. Whitesides, *Lab Chip*, 2014, **14**, 189–99.	Braille display is used to actuate elastomeric valves. Same principle could be also used to actuate paper valves based on cantilevers and push-button. This would allow automation of assays.	Electro-mechanical actuator / N/A / N/A	Phys	Operation / Reversible	Allows automation of paper devices with mechanical valves. Many channels. Can be reversible. No chemical interference.	Braille display is a more expensive component.
G. Korir and M. Prakash, *PLoS One*, 2015, **10**, 1–17.	Punch card and sound box can be used to actuate elastomer based microfluidic valves, but same principle could be also used to actuate paper valves based on cantilevers and push-button. This would allow automation of assays.	Multi-channel mechanical actuation program / N/A / N/A	Phys	Operation / Reversible	Allows automation of paper devices with mechanical valves. Many channels. Can be reversible. Low-cost and simple. No chemical interference.	No electronic control

Preparation of conductive paper for electrowetting

Electronically conductive paper was prepared by coating Whatman lens paper 105 with carbon ink. We prepared the carbon ink by dissolving carboxymethyl cellulose sodium salt (CMC, average M.W. 250'000g/mol, DS=1.2, obtained from Acros Organics) in de-ionized water (DIW) with a concentration of 10mg/mL. We added 300mg of multiwall carbon nanotubes (MWCNT, average outer diameter 6-9nm and length 5µm, obtained from Sigma-Aldrich, product code: 724769), to 10mL of the CMC solution and 20mL of DIW and dispersed the mixture for 15 min. using a Branson high-power sonifier 340, at a duty cycle of 50% and output power of 400W. The resulting ink was further diluted 50% in DIW. The lens paper was soaked into the ink solution; we used tissue papers to remove the excess ink and dried the lens paper in air. Subsequently, we hot pressed the lens paper at 210˚C for 1 min. to improve flatness. The properties of conductive paper for electrowetting are listed in table S2.

Table S2. Properties electrically conductive paper as a material for electrowetting.

Property	**Paper**
Initial Substrate	Whatman Lens paper 105
Conductive coating	Dip-coating with multi-wall carbon nanotube ink
Insulation layer	~10µm Parylene-C
Hydrophobic layer	Dip-coating with 0.2% solution of Teflon AF 2400
Resistivity (Ohm/sq.)	7700
Fiber diameter (µm)	~20
Opening size (µm)	~10 (large distribution)
Period (µm)	Non periodic
Thickness (µm)	45-50
Liquid breakthrough pressure (mbar)	12.6 ($\sigma = 3.8$)
Substrate cost (USD/cm^2)	0.00023

Parylene-C and Teflon coating of textiles and paper

The coating procedure was as follows: i) Samples were cleaned with a mixture of IPA:water (1:1) and primed with adhesion promoter Silquest A-17-NT silane (Chempoint, Bellevue, WA). ii) Samples were loaded in a deposition chamber, which was pumped overnight followed by coating at rate about 5µm/h. During coating samples were rotated in the chamber to improve thickness uniformity. Although the dimer precursor of parylene is pyrolized at high temperatures (680˚C) samples are not heated and stay at RT throughout the process. Thickness was estimated from deposition time and no online feedback was used. After completion, the thickness was measured on a sample piece and was found to be 11µm (target was 10µm). Parylene coating would be compatible with low-cost manufacturing. Due to large chambers one run (250USD) would allow production of material sufficient for a large number of devices.

Teflon AF 2400 (powder) and fully fluorinated solvent 3M Fluorinert® FC-40 were purchased from Sigma-Aldrich. A solution was prepared in a small glass jar, with Teflon® AF (w/w 1%). The jar was placed in a 50˚C water bath, and the mixture was stirred with magnetic stirrer for about 24h until complete dissolution. The 1% stock solution was further diluted into 0.2% solutions in the same solvent, and the textiles were dip-coated in this solution. The coated samples were dried first at ambient atmosphere for a minimum 15min, followed by 3h baking in an oven at 130˚C. Coatings of Si wafers (for contact angle measurement) was done using spin-coating at 4000rpm for 1min followed by same baking procedure.

Measurement of liquid breakthrough pressure for different textiles

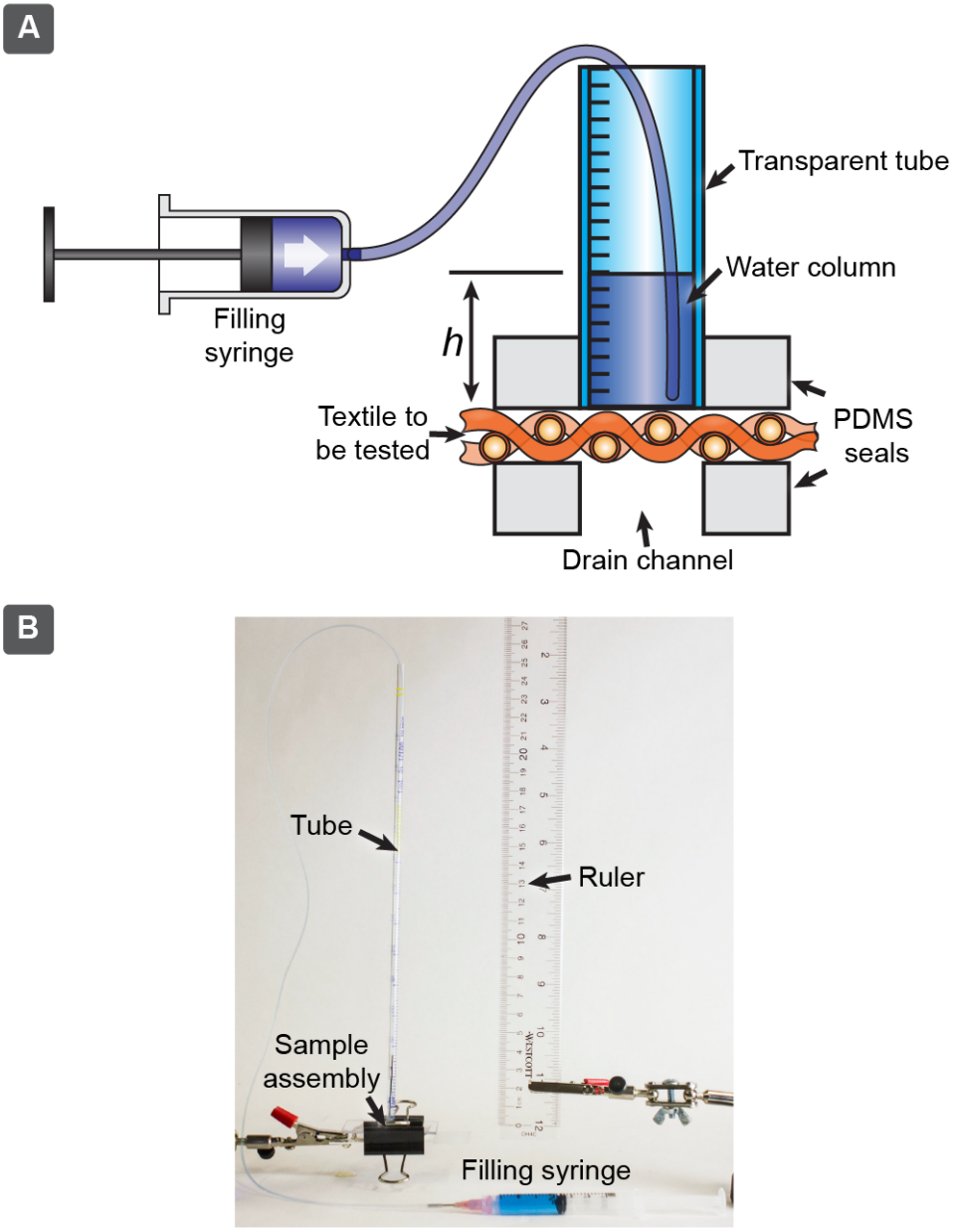

Figure S1. (A) Schematic diagram of a liquid breakthrough pressure measurement setup and (B) photo of it. As a transparent tube we used 10mL polystyrene serological pipette (I.D. 2.7mm). Measurement was carried out as liquid breakthrough into open drain channel.

Theory and basic characterization of electrowetting through textiles

To roughly describe this complex process with a simple model, we can consider the pressure p required for the liquid to pass through a porous material as given by the Washburn equation (Equation S1)

$$p = -\frac{4\sigma cos\theta}{d_p} \quad \text{(S1)}$$

here σ is surface tension of the liquid, θ is the advancing contact angle of the liquid on the surface of the porous material, and d_p is an average or effective diameter of the pore. Since the textile is hydrophobic ($\theta_0 = 105^{\circ}$), the pressure required to push a liquid through the textile is positive.

The contact angle θ can be modified via electrowetting (analogous to that of EWOD) by application of a voltage U according to the Lippmann-Young equation (Equation S2)

$$cos\theta = cos\theta_0 + \frac{\varepsilon\varepsilon_0 U^2}{2\sigma d_i} \quad \text{(S2)}$$

θ_0 is the initial Young's contact angle, ε is the dielectric permeability of the layer of insulation on the wires (3.15 for Parylene-C), and d_i is the thickness of the insulation layer (~10μm Parylene-C). Combining equation S1 and equation S2, we can see that an activation voltage U_a is required to trigger liquid flow through the textile (this happens when $p \approx 0$), according to (Equation S3).

$$U_a = \sqrt{-\frac{2\sigma d_i cos\theta_0}{\varepsilon\varepsilon_0}} \quad \text{(S3)}$$

To measure contact angles as a function of liquid surface tension, we used mixtures of ethanol (EtOH) and water to vary the surface tension in the range from 22mN/m (pure ethanol) to 72 mN/m (water), and measured the contact angle of the different mixtures as a function of applied voltage (Figures S3 A) on a Si-wafer coated with Parylene-C (11 μm) and Teflon AF. This data correlated well with equation 2 up to around 200 Volts (the Lippmann-

Young regime), but the contact angle did not change much as a function of voltage above 200V (this is known as the saturation regime). The deviation from theory in the saturation regime is not yet explained with a unified theory.

Next, we measured the actuation voltage for the different solutions on an aluminum textile coated with Parylene-C (11 µm), and Teflon AF (Figure S2). We could not determine an actuation voltage in case of 100% EtOH, since this solution penetrated through the textile without an applied potential. The highest EtOH concentration measured was 50%. Figure S4B shows the measured data vs. the theoretical value calculated from equation S3, using the material parameters $\frac{2\sigma_i d}{\varepsilon\varepsilon_0}$ where $d = 11\mu m$, $\varepsilon = 3.15$, $\sigma_i = 72\frac{mN}{m}(water)$, $56\frac{mN}{m}(5\%\ EtOH)$, $48\frac{mN}{m}(10\%\ EtOH)$, $29\ \frac{mN}{m}\ (50\%\ EtOH)$, and θ_0 is the initial Young's contact angle from the experimental measurements on planar surfaces.

We observed relatively large device-to-device variability in the minimal voltage threshold required to open a valve ("actuation voltage"), this is most likely due to the three dimensional nature of woven mesh combined with local variability in the thickness of coatings compare to, for example, planar EWOD devices. We also noticed that during the actuation the flow through the gate mesh starts at certain point or few points rather than through entire mesh instantaneously.

To summarize, we showed that the valves could function even for a liquid with an initial contact angle of θ_0=83˚ (surface tension 28mN/m). We derived a simple theoretical model (Equation S3) to calculate the threshold voltage of the valve actuation, and showed that this model works for estimating the actuation voltage but does not fully describe this system.

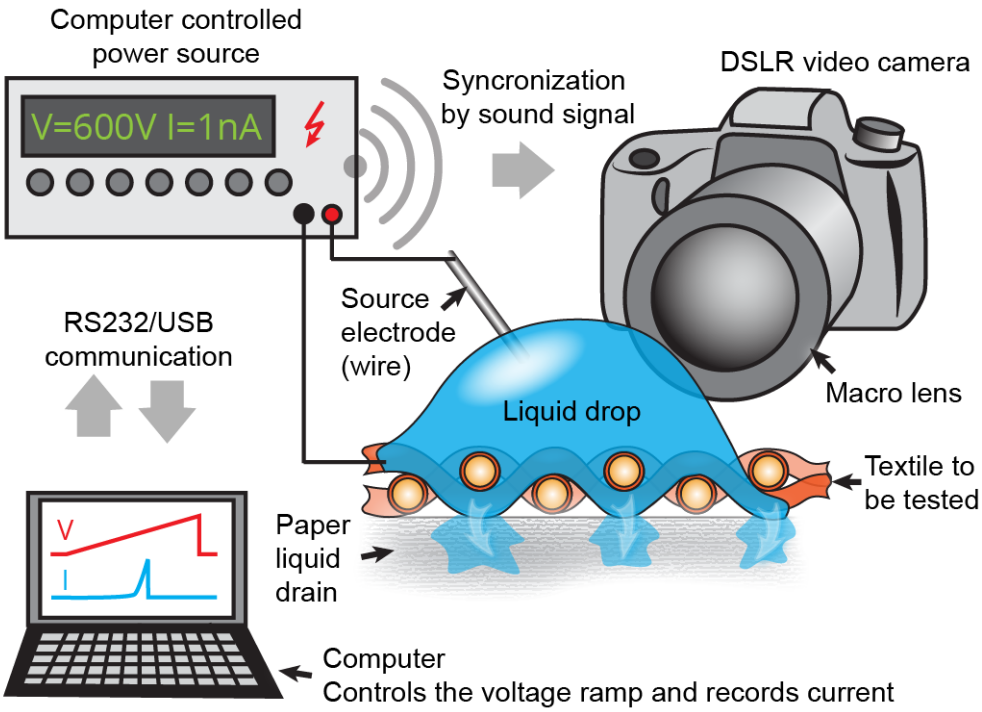

Figure S2. Experimental setup used to determine the actuation voltage of textile valves.

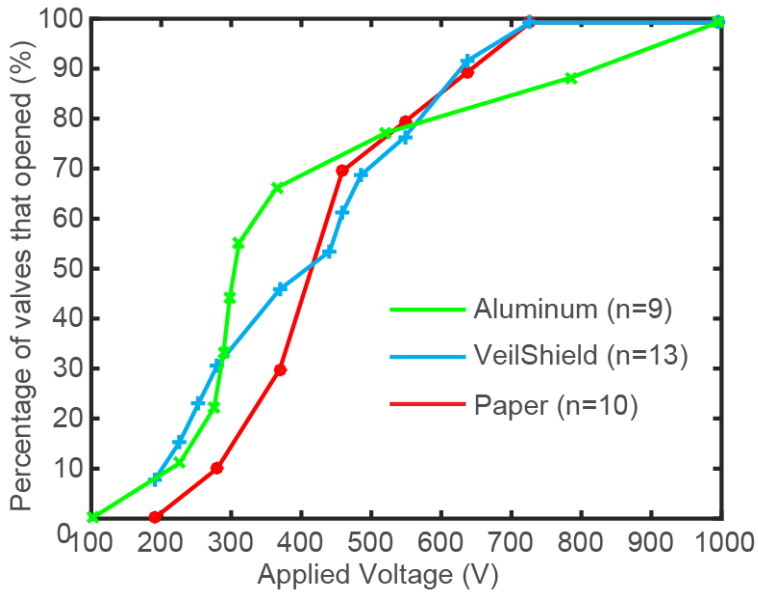

Figure S3. Percentage of valves (devices), which opened at certain voltage threshold, during the voltage ramp from 0 to 1000V. We tested the voltage response for three different materials: Aluminum, a plastic woven mesh with a conductive coating (see Table 1), and paper coated with a conductive carbon nanotube layer (see Table S2). Each material was tested for n different devices.

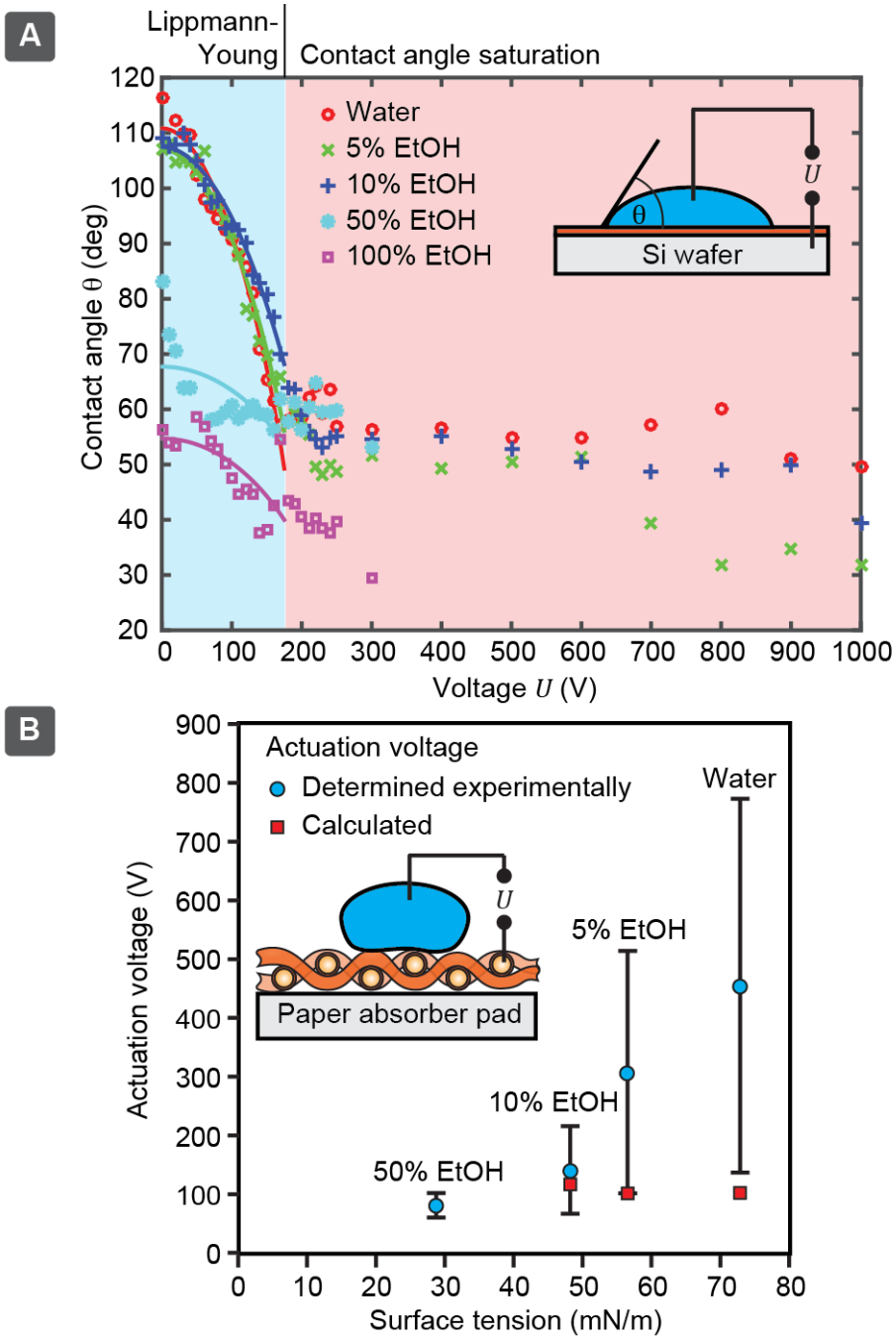

Figure S4. (A) Contact angle measurements of different EtOH solutions in water measured on Si-wafer with Parylene-C (10µm) and Teflon AF coatings. Contact angles at low-voltages (Lippmann-Young regime) were fitted to Lippmann-Young equation. (B) Actuation voltage of an aluminum textile with Parylene-C (10µm), and a thin Teflon AF coating, measured as a function of liquids with different surface tension, (water with different ethanol content). The theoretical values are calculated using equation S3.

Influence of ionic strength on the actuation voltage

We studied the dependence on ionic strength on the actuation voltage by using the same method and setup as described earlier. Here we used 20 µL droplets of 1 µM, 1 mM and 1 M KCl solutions to test the dependence of ionic strength on actuation. We could not observe any notable difference on DC actuation voltage in this concentration range as shown on Figure S5. This result is expected based on previous findings [Quinn et al. J. Phys. Chem. B 2003, 107, 1163-1169]. In these systems, the conductivity is expected mainly to affect the AC electrowetting [Kumar et al, Mater. Res. Soc. Symp. Proc. Vol 899, 2006]. We also did not observe any significant difference on the electrical current during valve actuation or the liquid flow rate through the valves.

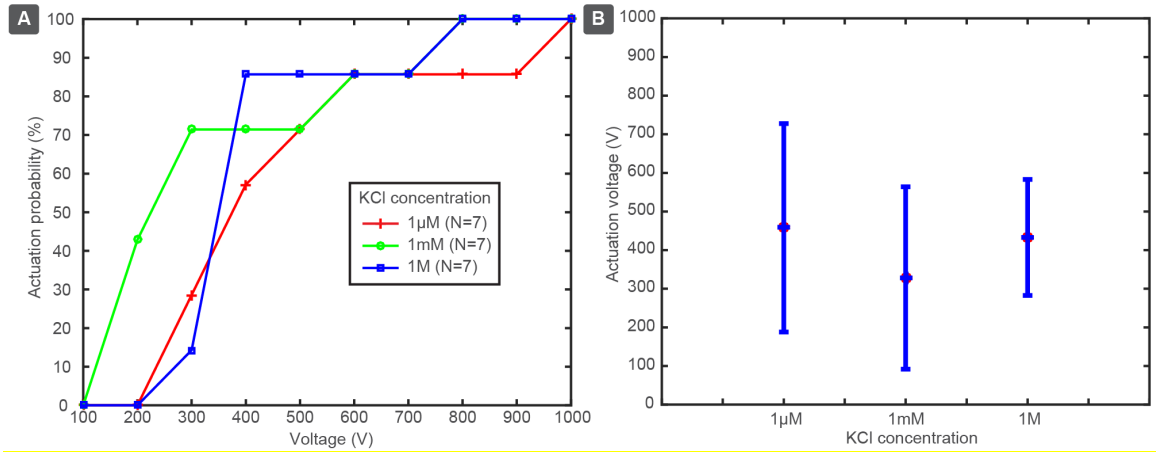

Figure S5. (A) The percentage of valves, which opened at certain voltage threshold during the voltage ramp from 0 to 1000V (N=7 devices). We measured the voltage responses for three solutions of varying ionic strength. (B) The average actuation voltage with standard deviation for the same experiment

Effect of the pulse length on valve actuation

To test the effect of pulse length on actuation, we used pulsed actuation voltage instead of a slowly ramped DC voltage. The electronic part of the setup was fabricated as shown on Figure S6A. We supplied an input voltage of 500 V and pulse-modulated the voltage using an N-CH MOSFET transistor FQN1N50CTACT (500 V, 380 mA). The gate of the transistor was controlled using a 80 MHZ arbitrary waveform generator Agilent 33250A, with digital signal output (levels 0 and 6 V). We varied the pulse length and number of pulses delivered. The Pulsing was triggered manually. We then monitored the flow rate of a coloured solution (Orange G in milli-Q water) into 5 mm diameter paper area with a camera Canon EOS (50 fps), and used a MATLAB based image analysis software to determine the filling time of the paper area as a measure of the valve opening. The filling was roughly proportional to the time after opening as seen on figure S6B. As a characteristic time-constant, we used the time required to fill the paper pad from 20 to 80%. In the first test we monitored 10 valves, while increasing the length of single voltage pulses in steps of 100 µs, 1 ms, 10 ms, 100 ms, 1 s. The 100 µs pulse was not able to trigger the valve, while the 1 s pulse triggered all valves (Figure S6C). Using shorter pulses yielded variable filling times (Figure S6D). There was, however, no clear correlation between the pulse length and the filling rate. Longer (1 s) pulses caused faster rate of filling. In a second test, we used 1 ms “on” 1 ms “off” pulses, but varied the number of pulses (5, 10, 20 pulses). Using sequence of 20 pulses yielded faster flow rate in all tests, with overall shorter control signal (total length of pulse sequence 40 ms). This result suggests that using pulsation could be efficient way to improve speed of opening of the valve, but using variable pulse length does not seem to be sufficiently reproducible to be exploited as a mean of control of flow rate.

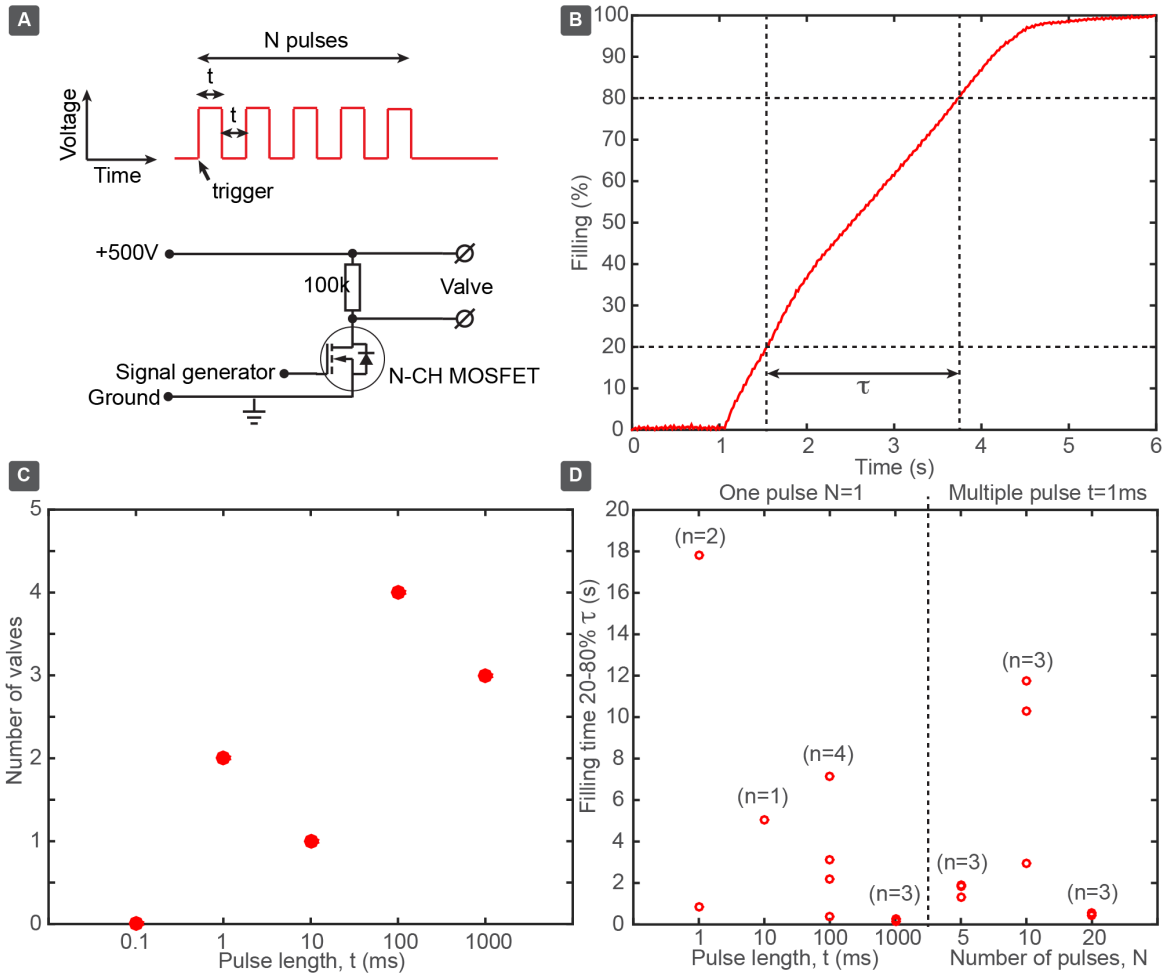

Figure S6. (A) The circuit diagram for pulse modulation device. (B) Filling of a 5-mm diameter paper pad, that is filled with a solution through a valve. (C) Minimal 500 V pulse length required to open the valve (n=10 devices). (D) Comparison of filling time depending on pulse length and number of pulses.

Textile valves as "electrofluidic thyristors"

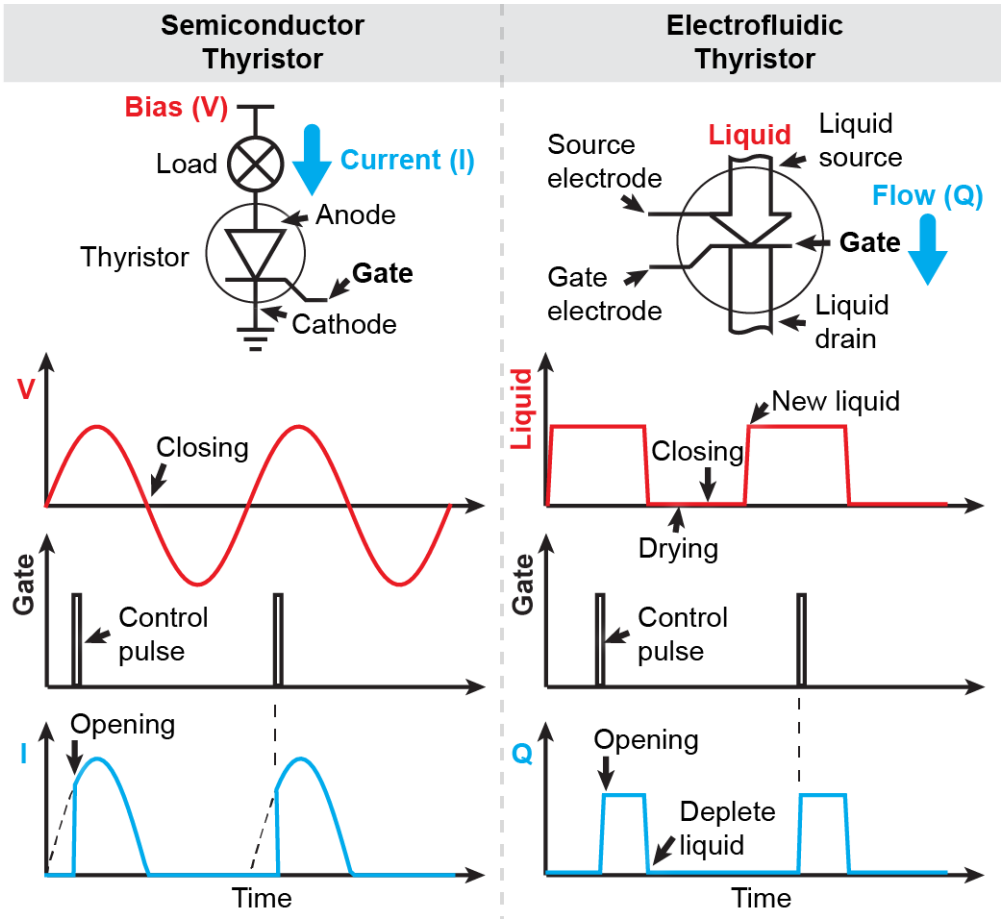

Figure S7. Schematic circuit diagrams and electrical function of a semiconductor thyrisor (left) vs. a fluidic thyrisor (right). Experimental repeated bistable actuation is demonstrated on following figure S8.

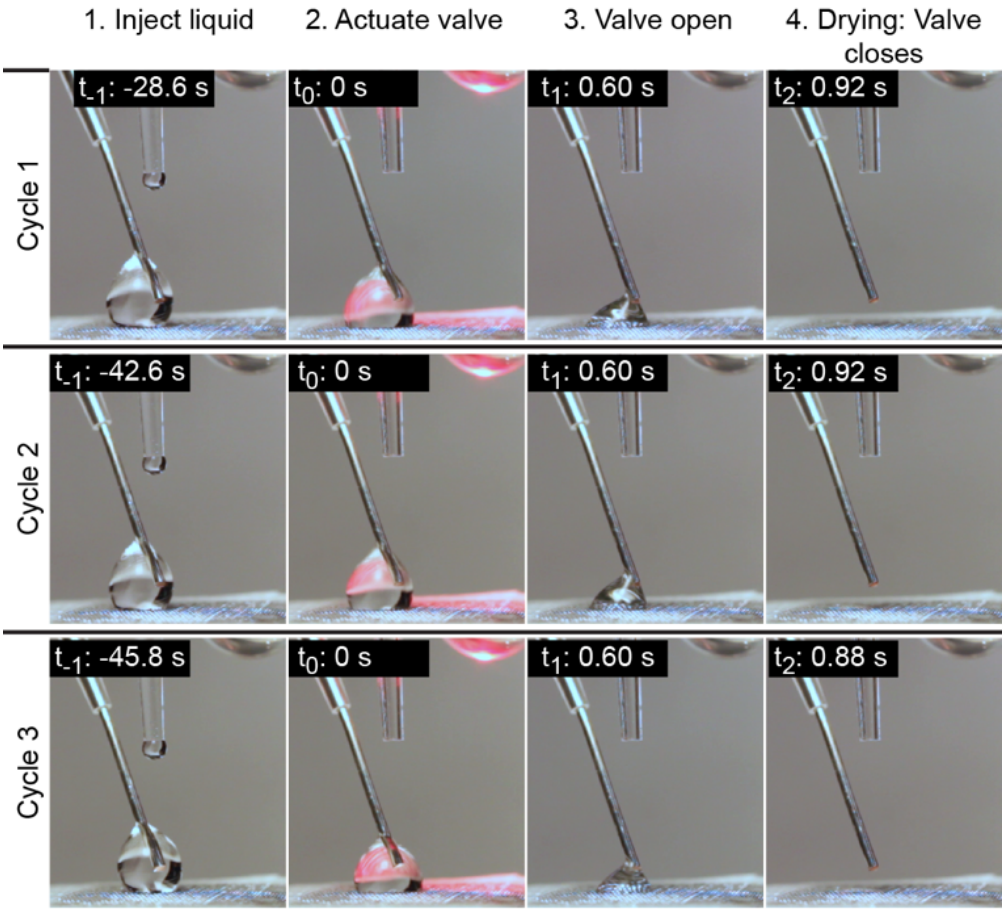

Figure S8. Time-lapse photos showing the function of a bistable electronically actuated liquid valve with three consecutive actuation cycles. Each cycle consists of: i) application of liquid (water), ii) opening of the valve with an electrical pulse, iii) liquid flow until the droplet has been depleted, and iv) drying of valve (restoration to the initial state).

Angle dependence

We tested valve actuation, when device is at different angles relative to the Earth ground. Since the angle cannot be changed in open textile configuration, as droplets would slide or drop off from the bare hydrophobic surface, we have embadded the textile (Aluminum) between two paper layers. Both paper layers had printed wax barriers surrounding circular hydrophic area (liquid source and drain. Source side is green and drain side is blue. Hydrophilic area had printed diameter 7.5mm). For electrical conductivity, source side had painted conductive ink electrode. Gate textile was directly connected with aligator clip. As a

liquid we used water, which was stained with acid red in order to facilitate visualization. Each time we loaded 20µL of liquid. We varied the angle from 0˚ (horizontal, droplet on top of paper) to 180˚ (upside down, droplet was hanging on the hydrophilic paper). All actuation voltages (Figure S9 A) were in the same range as measured at horizontal position (Figure S3B water), which is expected as capillary force is dominating over the gravity in case of small droplet (pressure from liquid column height is much lower than liquid breakthrough pressure)

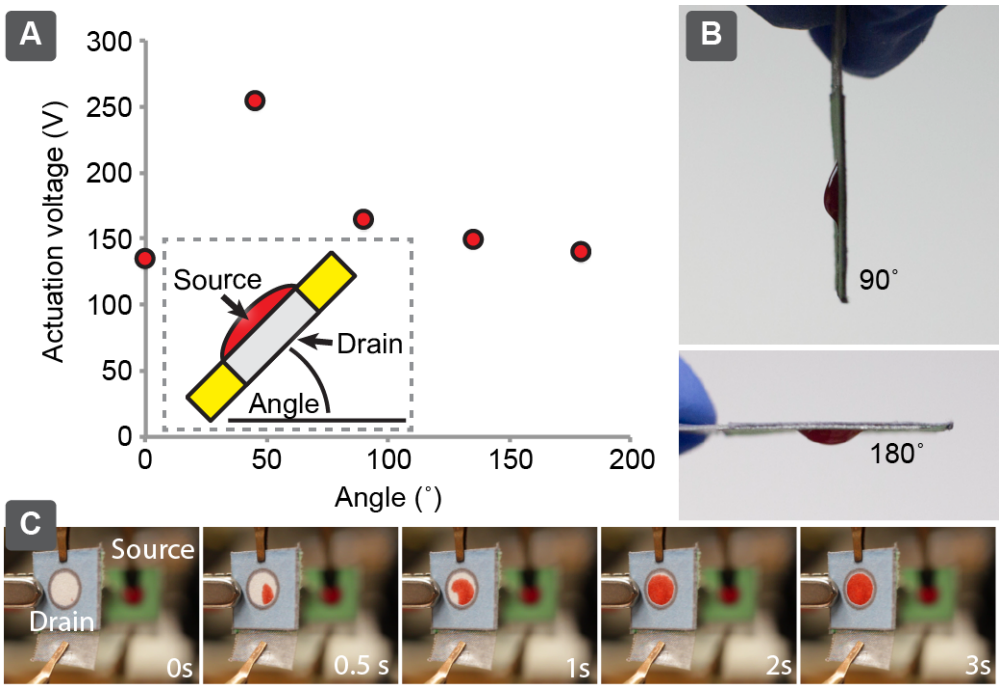

Figure S9. A) Measured actuation voltage depending on the angle. B) Liquid drop on the device source as seen at different angles. C) Exemplary time series of valve actuation at 90˚.

Logic control

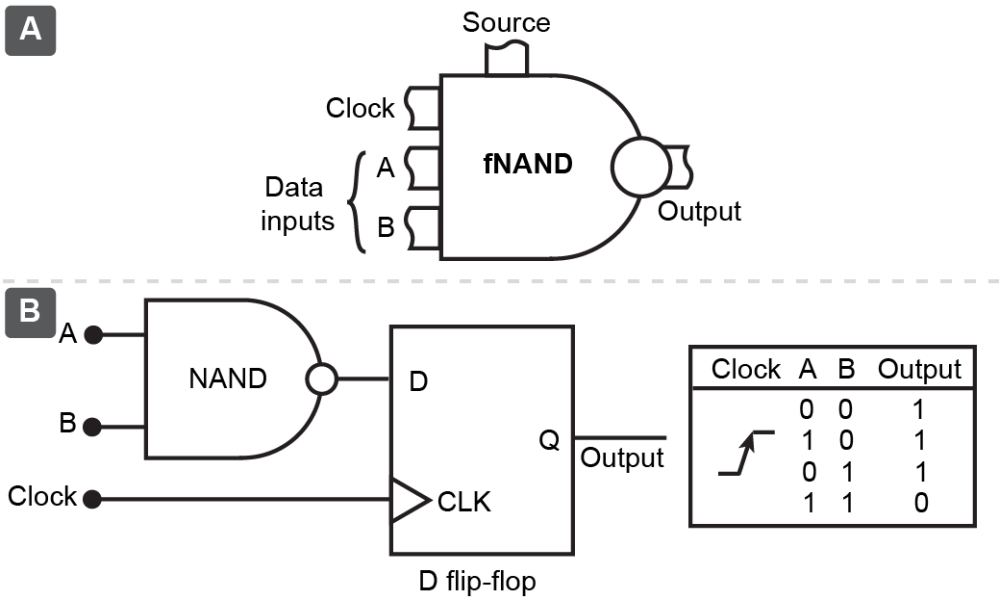

Figure S10. Fluidic NAND gate (fNAND) (A) Proposed symbol for fluidic fNAND. (B) Corresponding electronic equivalent scheme, which contains NAND gate and D flip-flop, and where the output of the NAND gate is coupled through the flip-flop.

Low-cost high-voltage power supply

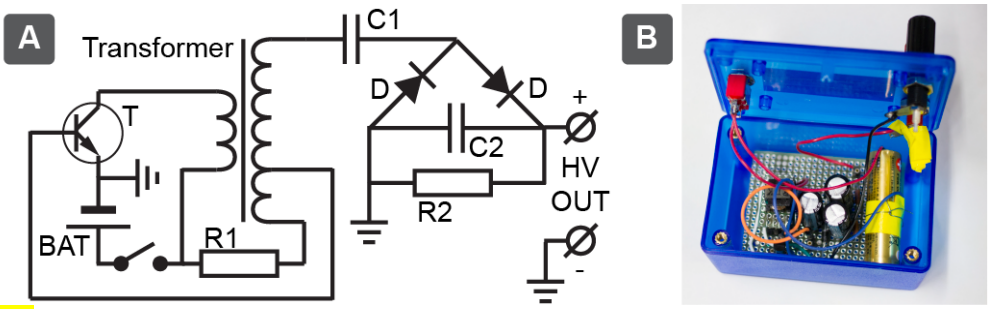

Figure S11. *High voltage at low-cost*. (A) Circuit diagram of a low-cost single-channel high voltage power supply sufficient to actuate the valves. We obtained all essential components of the power supply from the flash mechanism of Fujifilm disposable camera purchased from Amazon for 9.5USD. This circuitry was powered by a single AA battery (1.5V). Power supply contained following components: transformer (coil inductances 49µH, 100µH and 2H),

NPN transistor (D2504), two diodes (1N4007), capacitors (C1, C2: 10μF), and resistors (R1: 220Ohm, R2: 2MOhm). These were arranged functionally into a two-part oscillator with high-voltage transformer (Output: Vrms: 390V, 13kHz) and diode ladder/rectifier. The power supply had maximum output voltage of 650V and maximum current 3mA. The output voltage dropped linearly with current, giving internal resistance about 217kOhm. (B) Photo of the high voltage device. We measured the power consumption of the power supply. Approximately constant current 80mA was drawn from a single AA battery (1.5V). In an about 5s the output voltage reached 650V (Total energy from battery: 0.6J). At 100mA current load regular AA batteries (e.g. Energizer E91) have been specified to provide 2500mAh charge, which would correspond to 22320 charging (actuation) cycles.

Alternative high-voltage power supply design

We constructed another high voltage (HV) control unit (Figure S12) in order to automatically actuate multiple valves with high time resolution as well as to demonstrate a another feasible design approach for low-cost portable instrumentation. The key components of this design are a miniature HV converter (rendering 5V to 3kV) and high voltage transistors, enabling on-off switching of individual channels at voltages up to 4.5kV (This was the highest voltage rating commercially available, low-cost and miniature transistor we found). The purchased price of the HV converter and transistors was 138 USD and 15.3 USD/each, respectively. Thus the cost of the key components was about 170 USD. Remaining components were much cheaper or have low-cost alternatives (e.g. Arduino board (~45 USD) can be replaced with low-cost microcontroller with price less than a dollar). Price of HV components drops rapidly with voltage (e.g. for 1kV the material cost would be <100 USD and for 200V it would be <50 USD). This unit was based on microcontroller board Arduino Due, which was programmed in

C and powered and controlled through computer USB port. The computer side software was created in Visual Studio .NET C++.

The device was characterized and had following features:

- Two high voltage digital outputs able to switch between 0 and set HV level
- Capability to deliver HV pulses with 1ms time resolution (but accuracy is significantly higher).
- Manually or automatically adjustable HV level between 300V to 2.7kV (no load).
- Maximum output current 33μA (short circuit).
- For instrument safety, full galvanic isolation between low (LV) and high voltage electronics (HV converter is isolated internally and control signals were coupled from LV to HV side through optocoupler. HV side control was powered with individual small battery).
- Computer communication through USB emulated serial port.
- Synchronization output to trigger any other instrument (e.g. camera) or LED, which can be incorporated into visual field in case of video recording of valve operation and enables easier analysis of response

Materials. HV converter was purchased from EMCO High Voltage Corporation (Sutter Creek, CA). High voltage transistors were purchased from Mouser Electronics (Mansfield, TX). All other standard electronic components were obtained from Mouser Electronics, Digi-Key Corporation (Thief River Falls, MN) or were provided by Electronic Instrument Design Lab in Harvard University, Department of Physics. The detailed listing of components is brought in Table S3

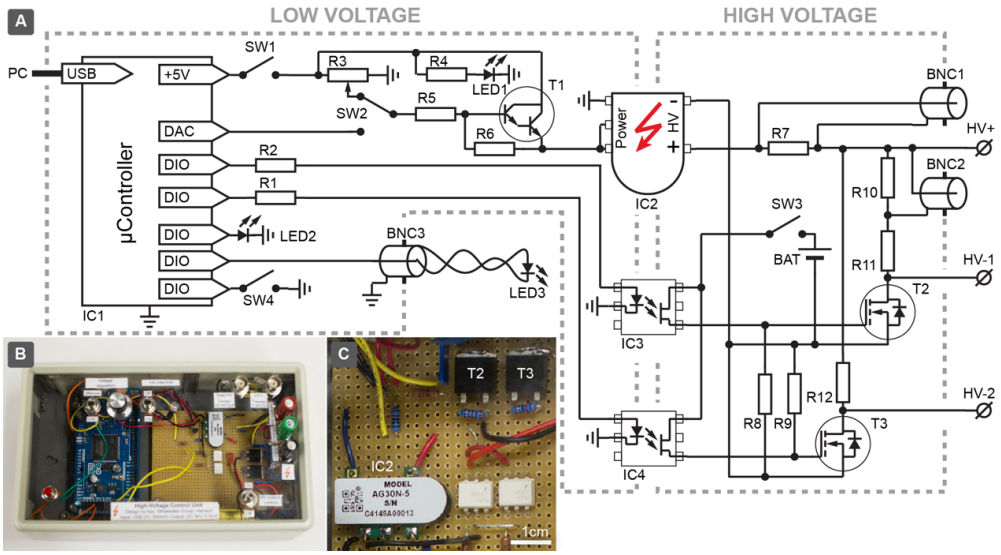

Figure S12. In-house built high voltage control unit. (A) Circuit diagram. (B) Photographs of a prototype device. (C) Photograph of the main parts of miniature high voltage electronics, showing 3kV high voltage converter (IC2) and 4.5kV FET transistors (T2 and T3). It shows that essential electronics could easily fit into a few cm sized portable module.

Table S3. List of components, for the high voltage device.

Component	Type/Value	Description
IC1	Arduino Due	Microcontroller board based on Atmel SAM3X8E ARM Cortex-M3 CPU (32-bit ARM core microcontroller). But can be also substituted with much lower cost controller.
IC2	EMCO AG30N-5	Miniature low to high voltage (HV) DC/DC converter (from 5V to 3kV). Input voltage 0.25-5V and current 200-470mA. Output voltage proportional to input in the range from 300V to 3kV with maximum output current 0.33mA and power 1W. Input and output side are galvanically isolated.
IC3, IC4	H11F1M	MOSFET optocoupler. Isolation voltage >5kV.
T1	2N6426	NPN Darlington transistor. Maximum current: 1.2A

		and amplification 20’000. For regulation of input voltage of HV converter.
T2, T3	IXTA02N450HV	n-channel MOSFET transistor. Maximum switchable voltage and current 4.5kV and 200mA. Gating threshold voltage: 4 to 6.5V Switching time <150ns.
SW1	Toggle switch	Powers HV circuitry. Safety interlock
SW2	Toggle switch	Switches voltage adjustment between manual and microcontroller regime
SW3	Toggle switch	Powers HV switching circuitry
SW4	Push button	For manual activation of output channel 1
HV+	Plug connector	HV output common terminal (+)
HV-1	Plug connector	HV output channel 1 terminal (-)
HV-2	Plug connector	HV output channel 2 terminal (-)
BNC1	BNC jack	Total HV current monitor 10mV/μA
BNC2	BNC jack	HV output channel 1 voltage monitor 1V/kV
BNC3	BNC jack	Synchronization output. For external electronics or LED
LED1	LED	HV power indicator. If “on”, HV converter is powered
LED2	LED	Microcontroller status indicator
LED3	LED	Synchronization LED (for video recording)
R1, R2	100 Ω	Optocoupler input LED current limiter
R3	1 kΩ	Adjustable potentiometer for manual voltage regulation
R4	1 kΩ	HV power LED current limiter
R5	1 kΩ	T1 transistor base current limiter
R6	10 kΩ	T1 transistor base pull down resistor
R7	10 kΩ	Current monitor resistor
R8, R9	10 kΩ	HV MOSFET pull down resistor
R10	1 MΩ	HV output channel 1 voltage monitor resistor
R11, R12	1 GΩ	HV output channel pull up resistor

BAT	PP3	9V battery for powering the HV switching circuitry for full galvanic isolation. Could be substituted with low-cost DC/DC converter.

Iodate Assay

Circular indicator pads (7mm diameter) were created using wax printing, as described before. 10 µL starch indicator was deposited on the pad and dried. First, we evaluated assay performance, by mixing the components in a test tube: 4µL of 1M p-toluenosulfonic acid, 2 µL of 0.5 M KI, 40 µL KIO_3 and 30 mM $Na_2S_2O_3$ solutions. We varied the KIO_3 concentration in series of 0, 0.1, 0.2, 0.5, 0.75, 1, 2, 3 and 5 mM and varied the volume of $Na_2S_2O_3$ in series 2, 4, 8 and 16 µL. After mixing, 10 µL of reaction product was transferred to the indicator pad. Visual change was recorded with a camera (Canon EOS 550D, EF-S 24 mm, and F2.8 lens). Colorimetric signal was evaluated using MATLAB, defined as a relative change in brightness (linear sum of individual RGB channels) of the indicator area. We then evaluated the storage of reagents in paper. Due to incompatibility, the input pad (circular 7mm diameter area) was divided into three equal sectors using 2pt line in Illustrator (a narrower line could not stop wicking). Same volumes of reagents were stored in these three sectors and dried in an oven at 60 ˚C until water had evaporated. First, we tested the assay without the valve by depositing 40µL of sample to the input pad, this amount of liquid was sufficient to cover the entire input pad and connect the individual sectors. Also since paper could not absorb the entire volume in its pores, an open drop left outside of the paper matrix would support convective mixing upon mechanical agitation. We used a custom built mechanical shaker shown in Figure S15. After 3 min of shaking, the reagent mixture was transferred to an indicator pad.

Table S4. Reaction can be limited by different components. If we denote the initial mole amounts of $K^+IO_3^-$, I^-, I_3^-, $S_2O_3^{2-}$ with *a, b, c, d* and end amounts with *A, B, C, D* respectively, we can calculate the end amounts of all reaction products or leftovers using the following equation systems. The amounts in the solution at the end must be equal to or larger than zero. Using the equations below, we can calculate the amounts at the end, for each initial combination.

	$K^+IO_3^-$ limited, I^- in excess	**$K^+IO_3^-$ in excess, I^- limited**
$S_2O_3^{2-}$ limited	$A = 0$ $B = b - 8a + \frac{3}{2}d > 0$ $C = 3a - \frac{1}{2}d > 0$ $D = 0$	$A = a - \frac{1}{8}b - \frac{3}{16}d > 0$ $B = 0$ $C = \frac{3}{8}b + \frac{1}{16}d > 0$ $D = 0$
$S_2O_3^{2-}$ in excess	$A = 0$ $B = b + a > 0$ $C = 0$ $D = d - 6a > 0$	Unphysical, as 8 I^- would give 3 I_3^- which each1 I_3^- would give further 3 I^- thus yielding +1 net effect, that can't be limiting, if other components are there.

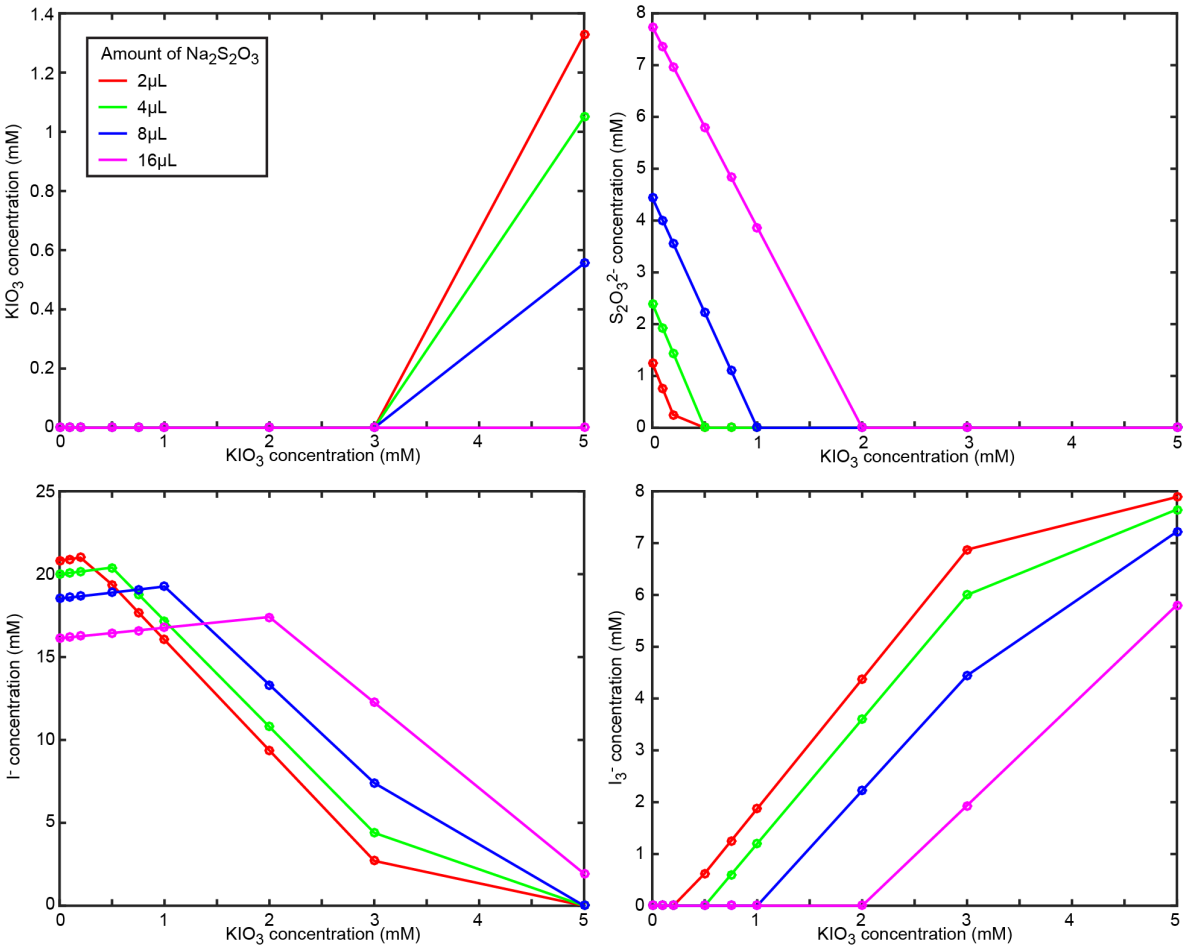

Figure S13. Calculated final amounts of all four compounds involved in the iodate assay reactions. All initial amounts correspond to the ones used in experiments described here.

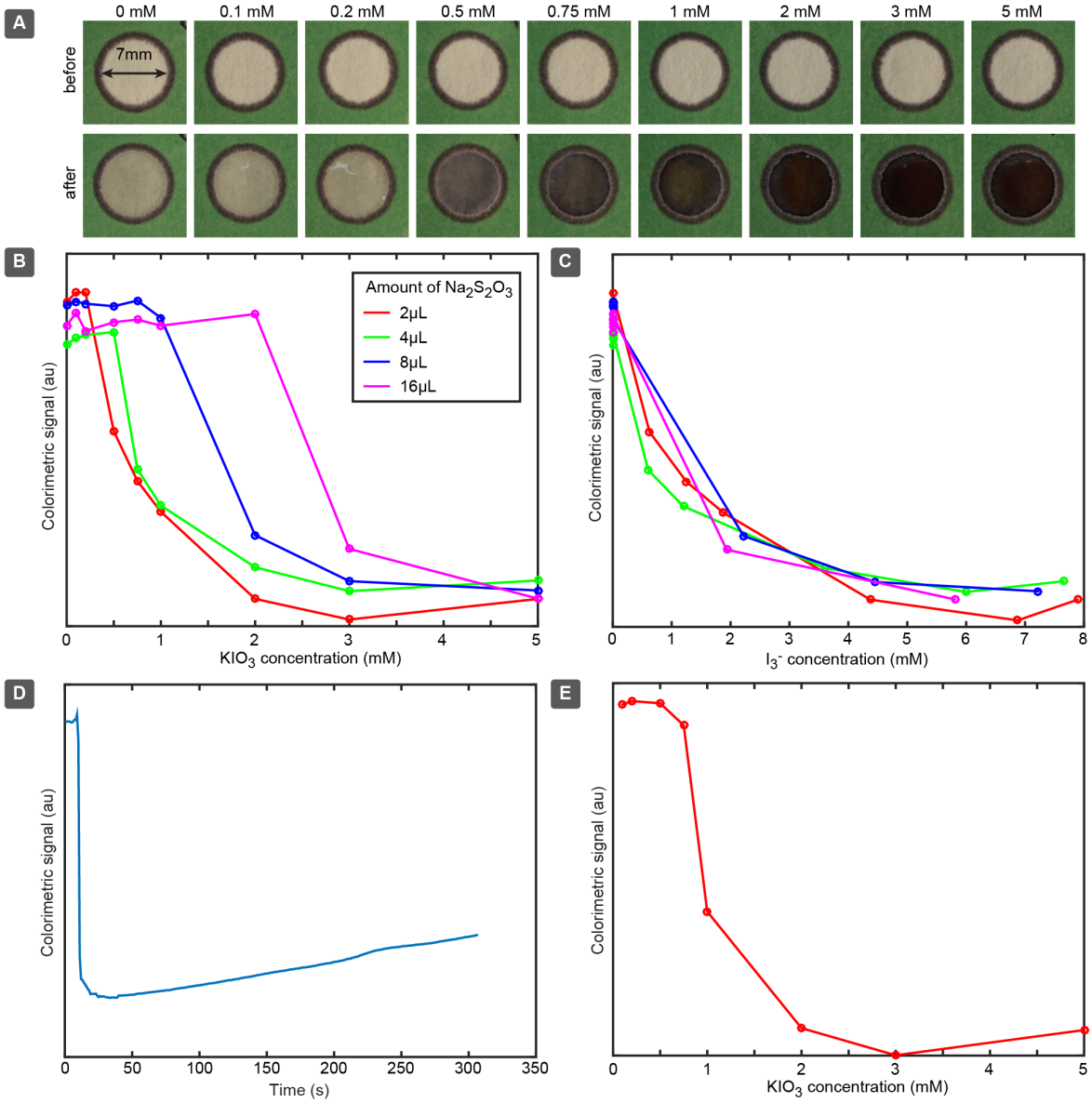

Figure S14. Experimental results: evaluation of starch indicator based colorimetric detection in the paper. First, the analyte and reaction components were mixed separately in test tube and product was added to the paper with starch indicator (A-D), thereafter we evaluated reaction, where components were stored in paper (E). (A) Image series of the visual appearance of the indicator area depending on analyte (KIO_3) concentration in the test mixture. (B) Colorimetric signal depending on analyte (KIO_3) concentration and amount of neutralizing $Na_2S_2O_3$. (C) Colorimetric signal depending on calculate concentration of I_3^- ion, which is forming dark blue complex with starch. (D) Time dependence of the colorimetric signal. Color is the darkest (Colorimetric signal value is lowest) directly after application of the sample, but it

recovers subsequently. (E) Assay evaluation where reagents are dried and stored in the paper (amount of $Na_2S_2O_3$ is 4 µL)

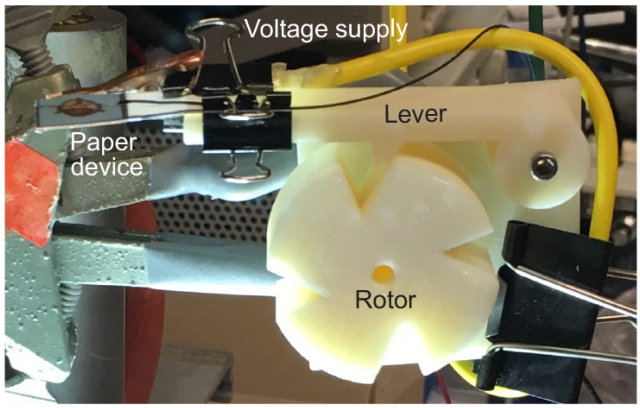

Figure S15. Photograph of a mechanical shaker. The rotor, lever and the assembly base were 3D printed. The rotor was driven by DC micro motor, at ~20 rpm. We used paper clips to attach the paper device and support wiring.

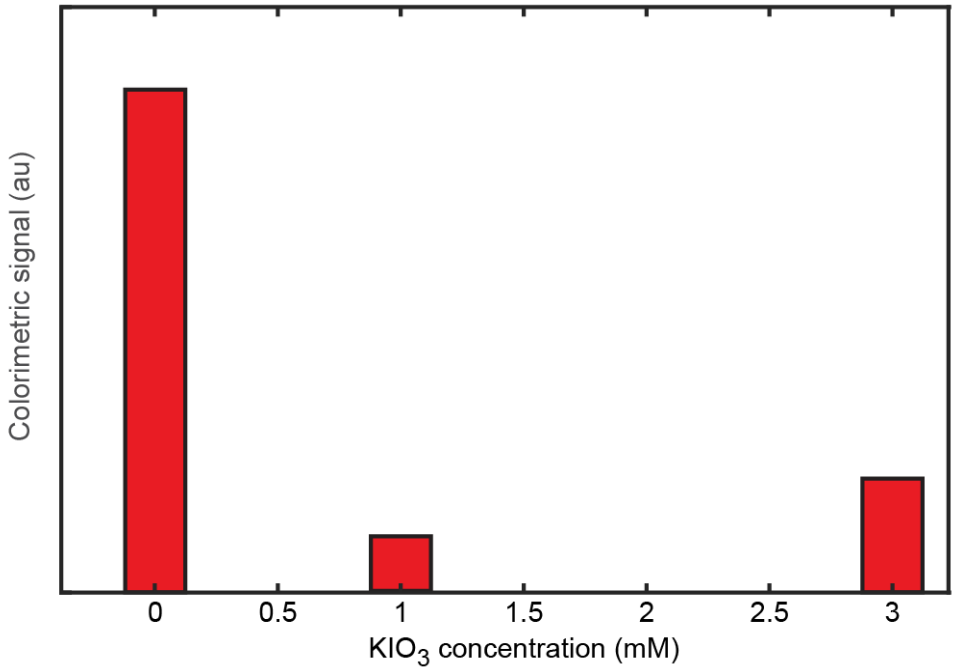

Figure S16. Experimental results showing colorimetric signal obtained for iodate assay with integrated valves.

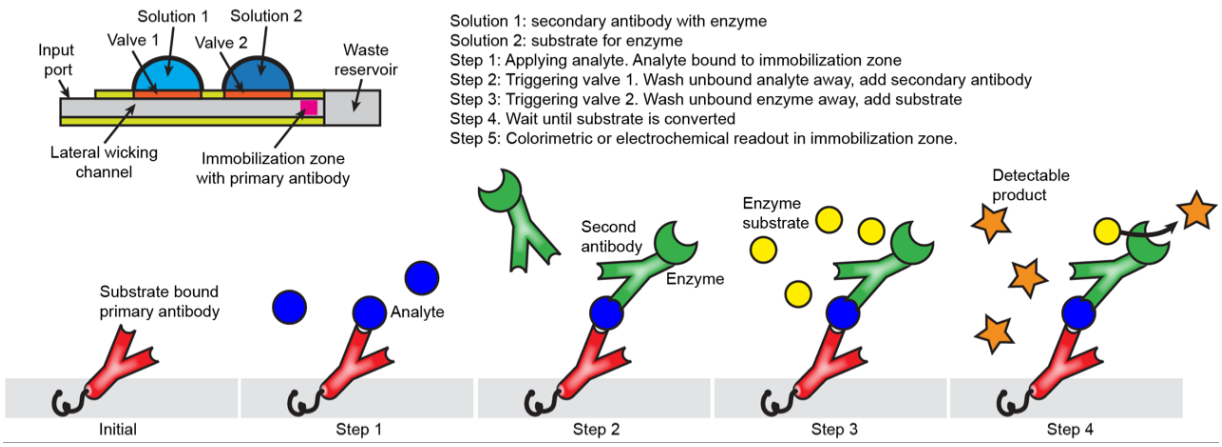

Figure S17. Schematic diagram showing one possible configuration that would integrate a paper-based ELISA assay in a lateral flow format, using two valves in a parallel configuration to automate the addition of reagents and the wash steps.